



RESEARCH ARTICLE

Multimodal MRI assessment for first episode psychosis: A major change in the thalamus and an efficient stratification of a subgroup

Andreia V. Faria¹  | Yi Zhao² | Chenfei Ye³ | Johnny Hsu¹ | Kun Yang⁴ | Elizabeth Cifuentes⁴ | Lei Wang⁵  | Susumu Mori¹ | Michael Miller⁶ | Brian Caffo⁷ | Akira Sawa^{4,6,8,9}

¹Department of Radiology, The Johns Hopkins University School of Medicine, Baltimore, Maryland

²Department of Biostatistics, Indiana University, School of Medicine, Indianapolis, Indiana

³Department of Electronics and Information, Harbin Institute of Technology Shenzhen Graduate School, Guangdong, China

⁴Department Psychiatry, The Johns Hopkins University School of Medicine, Baltimore, Maryland

⁵Department of Psychiatry and Behavioral Sciences and Radiology, Northwestern University, Evanston, Illinois

⁶Department of Biomedical Engineering, The Whiting School of Engineering, Baltimore, Maryland

⁷Department of Biostatistics, The Johns Hopkins University Bloomberg School of Public Health, Baltimore, Maryland

⁸Department of Neuroscience, The Johns Hopkins University School of Medicine, Baltimore, Maryland

⁹Department of Mental Health, The Johns Hopkins University Bloomberg School of Public Health, Baltimore, Maryland

Correspondence

Andreia V. Faria, Magnetic Resonance Research Division, Department of Radiology, The Johns Hopkins University School of Medicine, 217B Traylor Bldg., 720 Rutland Ave, Baltimore, MD 21205. Email: afaria1@jhmi.edu

Funding information

National Institute of Mental Health, Grant/Award Numbers: 094268, 092443, 105660, 107730

Abstract

Multi-institutional brain imaging studies have emerged to resolve conflicting results among individual studies. However, adjusting multiple variables at the technical and cohort levels is challenging. Therefore, it is important to explore approaches that provide meaningful results from relatively small samples at institutional levels. We studied 87 first episode psychosis (FEP) patients and 62 healthy subjects by combining supervised integrated factor analysis (SIFA) with a novel pipeline for automated structure-based analysis, an efficient and comprehensive method for dimensional data reduction that our group recently established. We integrated multiple MRI features (volume, DTI indices, resting state fMRI—rsfMRI) in the whole brain of each participant in an unbiased manner. The automated structure-based analysis showed widespread DTI abnormalities in FEP and rs-fMRI differences between FEP and healthy subjects mostly centered in thalamus. The combination of multiple modalities with SIFA was more efficient than the use of single modalities to stratify a subgroup of FEP (individuals with schizophrenia or schizoaffective disorder) that had more robust deficits from the overall FEP group. The information from multiple MRI modalities and analytical methods highlighted the thalamus as significantly abnormal in FEP. This study serves as a proof-of-concept for the potential of this methodology to reveal disease underpins and to stratify populations into more homogeneous subgroups.

KEYWORDS

DTI, factor analysis, first-episode psychosis, multimodal MRI, resting state fMRI, schizophrenia

This is an open access article under the terms of the Creative Commons Attribution License, which permits use, distribution and reproduction in any medium, provided the original work is properly cited.

© 2020 The Authors. *Human Brain Mapping* published by Wiley Periodicals LLC.

1 | INTRODUCTION

Although neuroimaging abnormalities in patients with first episode psychosis (FEP) have been demonstrated, their quantitative distribution is still under debate. Different patterns of atrophy in the frontal cortex, cingulate cortex, parahippocampal gyri, the basal ganglia, and the thalamus has been reported from multiple groups in the past (Buchy, Makowski, Malla, Joobar, & Lepage, 2018; Calvo, Delvecchio, Altamura, Soares, & Brambilla, 2019; Castro-de-Araujo & Kanaan, 2017; Kuang et al., 2017; Makowski et al., 2019; Nakamura et al., 2007; Schubert, Clark, & Baune, 2015; Tordesillas-Gutierrez et al., 2018). The inverse trend (gray matter increase) has also been reported (Dukart et al., 2017). Data in resting state functional MRI (rs-fMRI) that compare FEP patients with healthy controls (HC) are also controversial, varying from no differences between groups to regional or diffuse differences (Alonso-Solis et al., 2012; Argyelan et al., 2015; Bang et al., 2018; Choe et al., 2018; Ganella et al., 2018; Gohel et al., 2018; Huang et al., 2020; Tang et al., 2019). Previous observations of white matter changes have not been consistent. Differences in diffusion tensor imaging (DTI) were erratically reported in various brain areas such as the anterior limb of the internal capsule, the corpus callosum, the superior longitudinal fasciculus, and the uncinate. There was no specific cluster of white matter abnormalities that were unquestionably related to FEP (Deng et al., 2019; Di Biase et al., 2017; Kuswanto, Teh, Lee, & Sim, 2012; Lei et al., 2015; Ren et al., 2017; Serpa et al., 2017; Zhou et al., 2017). Recently, a large-scale study from the ENIGMA group identified widespread white matter microstructural abnormalities in chronic schizophrenia (Kelly et al., 2017). The reproducibility of this finding in individuals with FEP is still unknown.

The inconsistency of imaging study findings in FEP can be attributed to several factors. These include the inconsistency among studies regarding the actual definition of FEP (Breitborde, Srihari, & Woods, 2009), the limited power to detect subtle abnormalities in small samples (Buchy et al., 2018; Emsley et al., 2017; Guma et al., 2017; Kong et al., 2011; Kuang et al., 2017; Lee et al., 2012; Lian et al., 2018; McNabb et al., 2018; Peters et al., 2008; Serpa et al., 2017), as well as the bias in the selection of MRI modalities and regions of interest (ROIs) (Baglivo et al., 2018; Cho et al., 2019; Forns-Nadal et al., 2017; Huttlova et al., 2014; Lang et al., 2006; McHugo et al., 2018; Parellada et al., 2017; Sauras et al., 2017; Ublinskii et al., 2015; Vargas et al., 2018). Analyzing features through multiple MRI modalities over the whole brain became possible with the evolution of the scanners. Different neuroimaging modalities may capture different aspects of neuropathology and provide complementary information. The multimodal analysis reveals relationships between variables in imaging and nonimaging domains (e.g., genetics, cognition) and enables phenotypic characterization (Lerman-Sinkoff, Kandala, Calhoun, Barch, & Mamah, 2019; Moser et al., 2018; Tognin et al., 2020). The combination of multiple observables has already proven to be valuable in conditions affecting multiple systems, from financial markets (Kim, Min, & Han, 2006; Lessmann, Baesens, Seow, & Thomas, 2015) to cancer (Kourou, Exarchos, Exarchos,

Karamouzis, & Fotiadis, 2015), neurodegenerative diseases (Dai et al., 2012; Dyrba, Grothe, Kirste, & Teipel, 2015; Long et al., 2012; Zhang, Wang, Zhou, Yuan, & Shen, 2011), and psychosis (Schultz et al., 2012).

Schizophrenia is known to affect multiple domains (Fitzsimmons, Kubicki, & Shenton, 2013; Hirjak et al., 2019; Karlsgodt, Sun, & Cannon, 2010) and set up the ground for the initial attempts of multimodal analysis. (Aine et al., 2017; Calhoun & Sui, 2016; Meng et al., 2017; Shile et al., 2016; Sui, Huster, Yu, Segall, & Calhoun, 2014; Wang et al., 2015). Several recent studies have differentiated schizophrenia patients from HCs by combining data from functional and structural MRI (for a review, please see Rashid & Calhoun, 2020). They consistently found multimodal MRI classifiers more efficient than those based on single modalities (Cabral et al., 2016; Qureshi, Oh, Cho, Jo, & Lee, 2017; Yang, Liu, Sui, Pearson, & Calhoun, 2010). While these studies focused on patients with established diagnosis of schizophrenia, mostly far from the clinical onset, this assessment was not fully applied to study patients in initial stages of illness, when this characterization is likely to have greater utility. Patients with FEP were mostly assessed in with limited number of ROIs and few MRI modalities (Deng et al., 2019; Keymer-Gausset et al., 2018; Lei et al., 2015; Peruzzo, et al., 2015; Zhao et al., 2018).

Although its strengths, the implementation of this multimodal assessment is not straightforward: simply combining larger number of variables leads to multiple comparison issues and stress limitations of the sample size (Arbabshirani, Plis, Sui, & Calhoun, 2017). Multi-institutional brain imaging studies have recently emerged to overcome conflicting results among individual studies (Thompson et al., 2020). However, adjusting multiple variables at the technical and cohort levels remains a continuous challenge (Levin-Schwartz, Calhoun, & Adali, 2017). Developing strategies to reduce the dimensions of data, while preserving the information is a field in current development (Bassett, Xia, & Satterthwaite, 2018; Lottman et al., 2018; Miller, Vergara, & Calhoun, 2018; Qi et al., 2019; Sui, Adali, Yu, Chen, & Calhoun, 2012; Tu et al., 2019; Xia et al., 2018). A strong basis on biological knowledge is needed to develop and implement the algorithms in a comprehensive and practical way, so the research can eventually be translated to clinical field.

In order to overcome these challenges, we analyzed multiple MRI characteristics in the FEP and HC groups through whole-brain automated segmentation in a fully data-driven integrative approach that we have recently established (Miller, Faria, Oishi, & Mori, 2013; Rezende et al., 2019). This approach aims to reduce the dimensions of image data in a biologically meaningful way, increasing the statistical power and offering comprehensive results about the brain structure (Faria, Liang, Miller, & Mori, 2017; Miller et al., 2013; Mori, Oishi, Faria, & Miller, 2013). We combined this approach with supervised integrated factor analysis (SIFA) (Li & Jung, 2017) to examine multiple MRI features (volume, DTI indices, rs-fMRI) in the whole brain of FEP participants. We also accessed whether this multimodal approach would be efficient on classification of participants in subgroups of individuals with schizophrenia and schizoaffective disorder (S-FEP) and individuals with bipolar disorder and major depressive disorder with psychotic features (M-FEP). We investigated how this novel

analytical pipeline may provide evidence of pathological abnormalities in the early stage of illness and potentially aid to stratify groups of clinical relevance.

2 | MATERIALS AND METHODS

2.1 | Recruitment and participants

This study was approved and conducted using guidelines established by the Johns Hopkins School of Medicine Institutional Review Board and in accordance with The Code of Ethics of the World Medical Association (1964 Declaration of Helsinki). Each participant received a full explanation of the study procedures. Written informed consent was obtained for all participants 18 years of age and older. Parental consent and assent was obtained for all participants under 18 years of age. HCs and FEP patients, with FEP being defined as those who had experienced their first episode of psychosis within the 2 years prior to their enrollment, were recruited through the Johns Hopkins Schizophrenia Center. Details about the recruitment, inclusion and exclusion criteria, demographics, and clinical features are described in published articles by our group (Kamath et al., 2019; Kamath, Lasutschinkow, Ishizuka, & Sawa, 2018; Wang et al., 2019). In the present study, the participants included individuals with FEP ($n = 87$) [SZ ($n = 47$), schizoaffective disorder ($n = 14$), bipolar disorder with psychotic features ($n = 20$), major depressive disorder with psychotic features ($n = 6$)] and 62 HC. We included individuals with schizophrenia and schizoaffective disorder in the schizophrenia-associated psychosis group (S-FEP) and individuals with bipolar disorder with psychotic features and major depressive disorder with psychotic features in the mood-associated psychosis group (M-FEP). This decision was based on two meta-analyses (Pagel, Baldessarini, Franklin, & Baethge, 2013; Rink, Pagel, Franklin, & Baethge, 2016) that found patients with schizoaffective to have illness characteristics that align more closely with patients with schizophrenia than with those with bipolar disorder and major depression.

2.2 | Imaging

The multimodal MRI was performed on a 3 T scanner, and included T1 high-resolution-weighted images (T1-WI), diffusion weighted images (DWI), and resting state functional MRI (rs-fMRI). The image parameters were: (a) T1-WI: sagittal orientation, original matrix 170×170 , 256 slices, voxel size $1 \times 1 \times 1.2$ mm, TR/TE 6700/3.1 ms; (b) DWI: axial orientation, original matrix 128×128 , 70 slices, voxel size $0.83 \times 0.83 \times 2.2$ mm, TR/TE 8500/61 ms, 32 gradients, b factor $1,000 \text{ s/mm}^2$; and (c) rs-fMRI: axial orientation, original matrix 80×80 , 36 slices, voxel size $3 \times 3 \times 4$ mm, TR/TE 2000/30 ms, 210 time points.

We analyzed multiple MRI contrasts in an atlas-based, structurally focused, integrative, and non-biased whole-brain approach (Figure 1). The images were automatically segmented and postprocessed through MRICloud (www.MRICloud.org) (Mori et al., 2016), a public web-based

service for multi-contrast imaging segmentation and quantification. In MRICloud, the process for segmenting the T1-WI, used for volumetric analysis, involves: (a) orientation and homogeneity correction, (b) two-level brain segmentation, (c) image mapping based on a sequence of linear algorithms and Large Deformation Diffeomorphic Mapping (LDDMM), and (d) a final step of multi-atlas labeling fusion (MALF), adjusted by PICSL (Tang et al., 2013). For the DWI postprocessing, the tensor reconstruction and quality control follows the algorithm used by DtiStudio (www.MRIStudio.org). The automated DTI segmentation is similar to that used for T1-WIs and differs in the use of complementary contrasts (mean diffusivity [MD], fractional anisotropy [FA], and eigenvector such as fiber orientation) and a diffeomorphic likelihood fusion algorithm (Tang et al., 2014) for multi-atlas mapping.

For the rs-fMRI postprocessing (Faria et al., 2012), the T1-WI and its respective segmentations are co-registered to the motion and slice timing-corrected resting-state time points. Intensity and motion “outliers” are extracted with ART (SPM toolbox). Time courses are extracted from all the cortical and subcortical gray matter regions defined in the atlases and regressed for physiological nuisance. For “denoising” the time courses, we used the six motion parameters as regressors, as well as CompCor (Behzadi, Restom, Liu, & Liu, 2007) to regress nonneuronal physiological activity. These procedures, automatically performed in MRICloud, are similar to those adopted by major rs-fMRI postprocessing pipelines (e.g., SPM) and are detailed described in our previous publication (Faria et al., 2012). Furthermore, we calculated frame-wise displacement (FD) using six motion parameters (Power, Barnes, Snyder, Schlaggar, & Petersen, 2012). No participant had $FD > 0.5$, and only one participant had $FD > 0.3$. Both groups had small average values of head motion (mean $FD < 0.1$). Still, the FEP group showed larger FD than HCs ($p = .02$), justifying our procedure of using the motion-corrected time courses for the analysis. Seed-by-seed correlation matrices are obtained from the “nuisance-corrected” time courses and z-transformed by the Fisher’s method. Note that MRICloud pipelines include well accepted protocols to minimize artifacts, as those created by motion, in DWI and rsfMRI. These and other technical procedures are detailed in the original publications (Faria et al., 2012; Jiang, van Zijl, Kim, Pearlson, & Mori, 2006; Tang et al., 2014).

After the multimodal brain segmentation and quantification, each individual’s brain was represented by a vector of image features: (a) volumes of 198 structures automatically segmented from T1-WIs, (b) fractional anisotropy (FA) and (c) mean diffusivity (MD) means of 96 structures automatically segmented from DTIs, and (d) 2415 pairwise resting-state z-correlations from 70 seeds in the superficial gray matter (i.e., cortex) and the deep gray matter (i.e., basal ganglia plus thalamus). This process is represented in Figure 1.

2.3 | Statistical analyses

We investigated group differences between FEP groups and HC (HC vs. FEP, HC vs. S-FEP, and HC vs. M-FEP) in the various imaging modalities by using two-sample *t* tests. The False Discovery

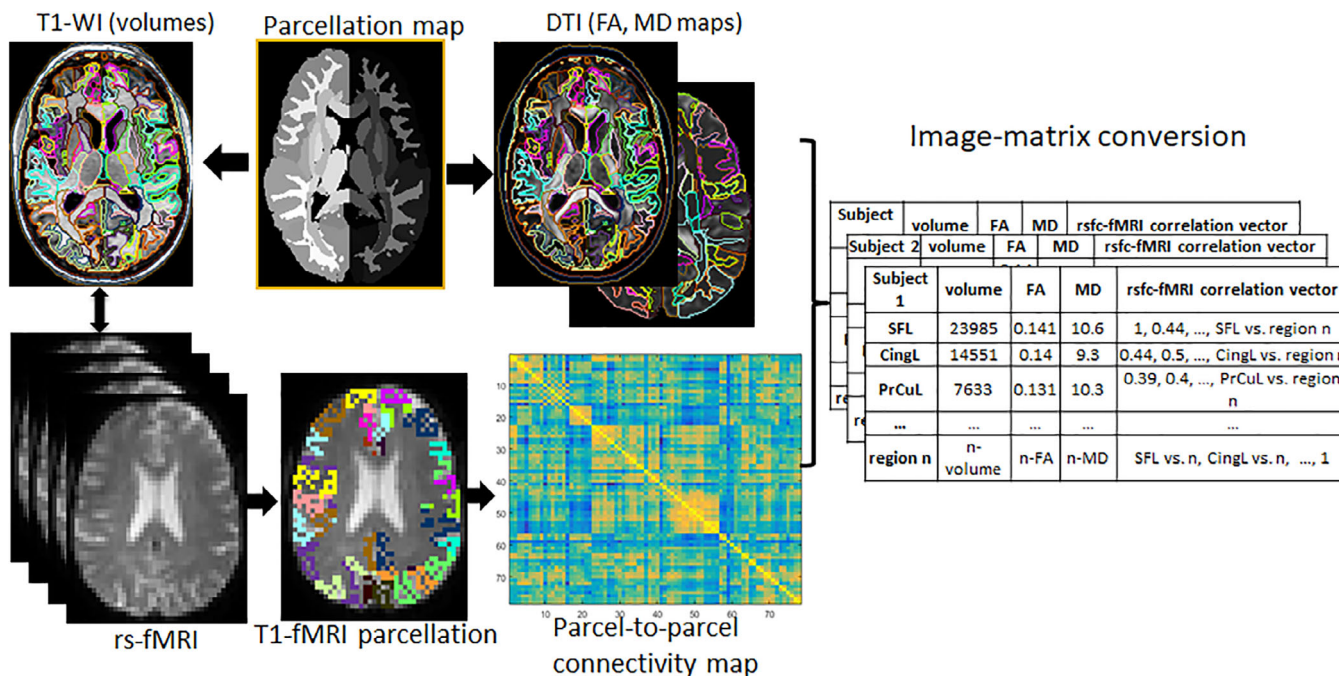


FIGURE 1 Schematic representation of the automated image parcellation using MRICloud (www.MRICloud.org). Each brain image is mapped to a set of multiple atlases and the pre-defined labels are applied to each original brain. T1-weighted images (for volumetric analysis) and DTI pipelines run in parallel. For the low-resolution modalities (e.g., rs-fMRI), the labels are brought to the original space by co-registering the T1-WIs. Through this process, the multiple MRI modalities are converted to a matrix of structures by image features, which represent each individual

Ratio (FDR) (Benjamini & Hochberg, 1995) was used to correct for multiple comparisons at a “ q ” (“ p -corrected”) level of significance $<.05$.

The SIFA was implemented to integrate data collected from multiple imaging modalities while facilitating characterization with auxiliary covariates. For each modality, it is assumed that the data consist of two types of latent factors: (a) common factors shared across all modalities and (b) individual factors specific to the data source. For both types of latent factors, a linear regression model of the covariates was used to capture the influential effects. Since the goal of implementing SIFA is to integrate multiple imaging modalities and identify joint structure, we only present the results of the estimated common factors. The latent factors are assumed to be independent, which is analogous to the assumption imposed in the independent component analysis (ICA) (McKeown & Sejnowski, 1998) widely used in neuroimaging analysis. The ranks of the factors were chosen based on a likelihood cross validation (LCV) approach. Similarly to what is done in a sparse principal components analysis (Zou, Hastie, & Tibshirani, 2006), loading profiles were sparsified through a penalized regression to achieve the purpose of feature selection. The covariates for adjustment included group (FEP, HC, S-FEP, M-FEP) as well as race, sex, and age. Because in our study the data dimension is slightly unbalanced among modalities, we implemented the “SIFA-B” approach (Li & Jung, 2017), which is robust to unbalanced dimensions due to orthogonal and

equal norm identifiability conditions. To test the significance of the coefficients in the regression models, confidence intervals were obtained using 500 bootstrap samples. Details about SIFA, the procedure to draw inference, and the classification approach are in Section A of the Supplementary material.

While group features may reveal pathological mechanisms, it is important to know if the multimodal features revealed by SIFA are expressed at an individual level. Therefore, we investigated the power of these image features to classify individuals within their respective diagnostic groups. It is also important to detect the effectiveness of models using multiple modality features, as compared with those using singular modality features for individual classification. For this purpose, we used leave-one-out cross-validated receiver operating characteristic (ROC) curves. The logistic classification models were trained using the latent factors estimated from the factor analysis. The area under the curve (AUC) and the 95% confidence interval were calculated. We also calculated the sensitivity, specificity, and F1 score of the classification performance using the latent factors estimated from SIFA. We compared the performance with the support vector machine (SVM) approach considering three different types of kernel functions: linear, polynomial and radial kernels. For all approaches, five sets of data were considered to train the prediction model: (a) data of all modalities, (b) rs-fMRI data, (c) FA (from DTI), (d) MD (from DTI), and (e) T1-volumetric data. The data analyzed in this study and the analytical code are available under request to the authors.

3 | RESULTS

3.1 | Demographic analysis

Clinical and demographic variables are presented in Table 1. Since covariates were group-matched based on study design, the FEP group, its subgroups, and the HC group did not differ with respect to age, sex, race, and parental education. The FEP subgroups did not differ in illness duration and antipsychotic medication dosage.

3.2 | Group comparison (FEP vs. HC) of imaging characteristics in each modality

No volumetric differences were found between FEP and HC groups after the multiple comparisons correction. With respect to DTI differences, FEP individuals showed lower FA in the global white matter (defined as the average of all white matter segments) as compared with HC. More specifically, FEP and HC groups differed in DTI indices (FA and MD) in most subsegments of the projection fibers (cortico-spinal and spino-cortical). These fibers represent most of the motor and sensorial tracts. These two groups also differed in MD and FA at the main commissural fibers, as represented by the corpus callosum (Figure 2, Table 2). Association areas also showed abnormal DTI indices. Compared with the HC group, the FEP group showed lower FA and higher MD in the corona radiata and the inferior fronto-occipital fasciculus; lower FA in the white matter beneath the right superior frontal gyrus; as well as higher MD in the uncinate fasciculus, cingulum, and in the white matter beneath the inferior temporal and middle and inferior frontal gyri. In the deep nuclei, FEP showed lower FA in the globus pallidus, higher FA in the caudate, and higher MD in the thalamus and the putamen when compared with HC.

With respect to rs-fMRI differences, the FEP group showed higher rs-fMRI z-correlations than the HC group between several pairs of regions. Regions most often detected as seeds of abnormal correlations were the thalamus, the cerebellum, the somato-sensorial cortex (parietal, post- and pre-central), and the cingulate cortex (Figure 2, Table 2).

3.3 | Subgroup comparison (S-FEP and M-FEP vs. HC) of imaging characteristics in each modality

Given that the FEP group and the HC group display anatomical differences, we next addressed the possible FEP subgroup that might contribute most to these differences. As described in the Methods section, we subdivided the FEP subjects into S-FEP and M-FEP groups and compared these individual groups with the HC group.

The differences detected between S-FEP and HC were more widespread and had a higher effect size than those detected between FEP and HC. This is of great importance, considering the fact that S-FEP is a subset, and therefore a smaller group than the more general FEP group. Volumetric differences did not overcome the

TABLE 1 Demographic and clinical characteristics

	Mean ± SD [min max]		p-value (T or χ^2 statistic)					
	HC (n = 62)	All FEP (n = 87)	S-FEP (n = 61)	M-FEP (n = 26)	HC vs. FEP	HC vs. S-FEP	HC vs. M-FEP	S-FEP vs. M-FEP
Age (years)	23.4 ± 3.6 [16 33]	22.5 ± 4.3 [15 35]	22.3 ± 4.2 [15 34]	23 ± 4.8 [17 35]	0.16 (-1.4)	0.16 (-1.5)	0.64 (-0.46)	0.57 (-0.57)
Sex (M:F)	43:19	53:14	49:12	14:12	0.82 (0.04)	0.82 (1.4)	0.25 (1.3)	0.02 (5.1)
Race (aa:c:as:h:o)	33:23:2:2:2	43:34:4:3:3	33:23:2:1:2	10:11:2:2:1	0.85 (0.03)	0.85 (1)	0.52 (0.39)	0.52 (0.4)
Parental education (years)	15.18 (2.62)	15.1 ± 3.2	14.96 (3.06)	15.42 (2.63)	0.84 (0.03)	0.51 (0.4)	0.73 (0.25)	0.65 (0.36)
Age at onset (years)			21.3 ± 4.1 [14 32]	22.3 ± 4.7 [15 34]				0.35 (-0.92)
Illness duration (months)			13.2 (8.9)	10.8 (9.5)				0.3 (1)
Antipsychotic dose ^a			381.9 ± 302.9	267.3 ± 221.5				0.07 (1.8)
SAPS			3.9 ± 3.7 [0 15]	2.2 ± 3.7 [0 12]				0.06 (1.9)
SANS			8.5 ± 5.0 [0 20]	4.4 ± 4.4 [0 16]				0.0004 (3.7)

Note: Race codes: aa, African American; as, Asian; c, Caucasian; h, Hispanic; o: others.

Abbreviations: HC, healthy controls; M-FEP, major depression and bipolar disorder with psychiatric features; SANS, Scale for the Assessment of Negative Symptoms; SAPS, scale for the assessment of positive symptoms; S-FEP, schizophrenia and schizoaffective disorders.

^aAntipsychotic medication dosages were converted to chlorpromazine equivalents using published reference tables (Woods SW. Calculation of CPZ Equivalents. In: Equivalent C, ed. 2005). Medication dosage information was unavailable for six patients.

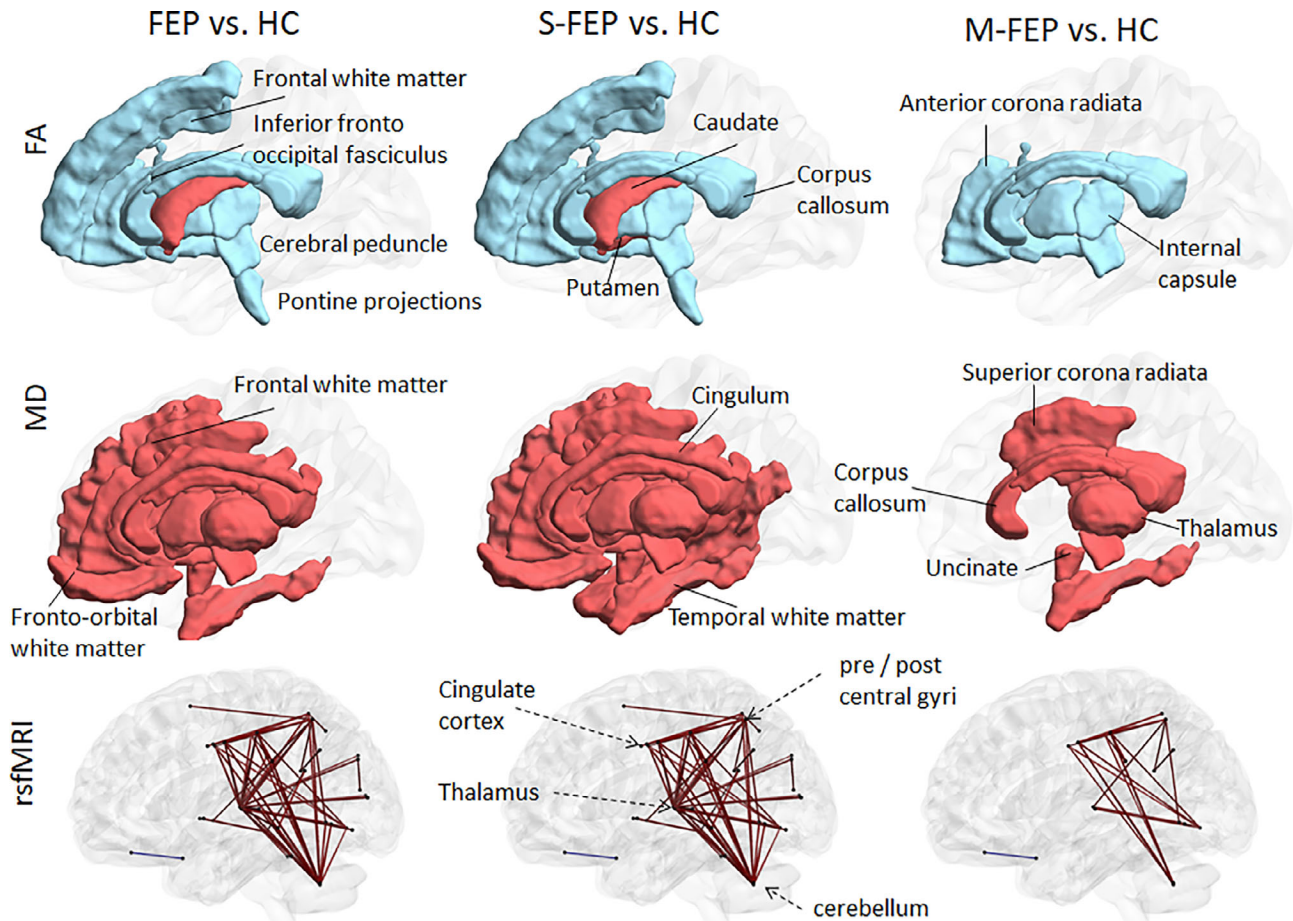


FIGURE 2 Differences in imaging features between groups. Regions with abnormal DTI indices [FA (top row), MD (middle row)] and edges of abnormal rs-fMRI synchrony (bottom row) in FEP (left column), S-FEP (middle column), and M-FEP (right column) compared with HC. Blue are lower mean values in FEP groups compared with controls; red are higher mean values in FEP compared with controls. Visualization with the BrainNet Viewer (<http://www.nitrc.org/projects/bnv/>, by Xia, Wang, & He, 2013)

threshold for multiple comparison correction, possibly due to the inclusion of individuals in early disease stage, whose brain structure was under minimum effect of the treatment and disease chronicity (van Erp et al., 2016; Vita, De Peri, Deste, Barlati, & Sacchetti, 2015). Yet, the S-FEP group tended to have a larger Sylvian fissure ($p = .028$) and cingulum sulci ($p = .027$) than HC. This indirectly indicated possible atrophy or anatomical abnormalities of the adjacent structures (planum temporalis, insula, and cingulum), a progressive feature of psychotic brains (Kasai et al., 2003; Lee et al., 2016; Rosa et al., 2015). In addition to what was observed in the FEP versus HC comparison, the DTI abnormalities spread to the putamen and the white matter beneath middle temporal (Figure 2, Table 2). The rs-fMRI abnormalities had, in general, a higher effect size than in the FEP versus HC comparison (Table 2).

No differences in volume were detected between M-FEP and HC. Differences in DTI and rs-fMRI between M-FEP and HC were more constrained to a few regions and had a lower effect-size than those observed between S-FEP and HC (Figure 2, Table 2).

3.4 | Multimodal characterization (SIFA) of FEP group

Given that the group comparison in the present study still involved many features from multiple MRI modalities (hundreds of volumes and DTI indices, and thousands of rs-fMRI), we next applied SIFA for data integration. As described in the Materials and Methods section, SIFA allows us to identify the latent factors (i.e., the combination of features) related to the different groups, as well as leverage information across modalities.

SIFA identified two common latent factors as different between FEP and HC; one factor in the S-FEP versus HC comparison, and one factor in the M-FEP versus HC comparison. The weights (sparsified loadings) of these factors are shown in Figure 3 and Table 3. The corresponding model coefficients and the 95% bootstrap confidence intervals are in Supplemental Figure S1. Common features of the latent factors were identified in each of the different comparisons (e.g., FA of body of the corpus callosum, the inferior fronto-orbital

TABLE 2 Group differences

		Group means				HC vs. FEP		HC vs. S-FEP		HC vs. M-FEP	
		HC	FEP	S-FEP	M-FEP	T	p-value	T	p-value	T	p-value
Fractional anisotropy—FA											
Projection	Cerebral peduncle	0.670	0.653	0.654	0.649	-6.065	.000	-4.853	.000	-5.773	.000
	Pontine projections	0.552	0.539	0.536	0.545	-4.310	.000	-4.595	.000	-1.747	.084
	Post limb int capsule	0.636	0.626	0.626	0.628	-3.555	.000	-3.409	.001	-2.097	.039
	Ant limb int capsule	0.570	0.559	0.560	0.556	-3.894	.000	-3.234	.001	-3.066	.003
	Corpus callosum	0.610	0.593	0.597	0.585	-5.715	.000	-3.900	.000	-7.694	.000
Assoc.	Inf frontoccipital fasc	0.445	0.435	0.438	0.430	-2.958	.003	-2.050	.042	-2.842	.006
	Ant corona radiata	0.433	0.427	0.428	0.425	-2.334	.020	-1.731	.045	-2.228	.029
	Sup frontal WM	0.384	0.381	0.380	0.381	-2.114	.035	-2.153	.032	-1.130	.261
Nucleae	Caudate	0.220	0.233	0.236	0.223	3.633	.000	3.881	.000	0.825	.412
	Globus pallidus	0.378	0.363	0.362	0.364	-2.221	.027	-2.184	.030	-1.341	.183
	Putamen	0.230	0.238	0.239	0.233	1.881	.061	2.040	.043	0.551	.583
	Total white matter	0.456	0.452	0.453	0.450	-2.863	.005	-1.999	.047	-2.924	.005
Mean diffusivity—MD ($\times 10^{-4}$, in mm^2/s)											
Project.	Cerebral peduncle	8.707	8.932	8.922	8.956	3.910	.000	3.424	.001	3.083	.003
	Ant limb int capsule	7.553	7.713	7.748	7.631	3.330	.001	3.717	.000	1.077	.285
	Post limb int capsule	7.200	7.313	7.307	7.325	2.700	.007	2.386	.018	2.041	.044
	Corpus callosum	9.280	9.552	9.562	9.528	5.444	.000	5.400	.000	2.962	.004
Association	Sup corona radiata	7.340	7.462	7.473	7.436	3.710	.000	3.603	.000	2.213	.029
	Ant corona radiata	8.441	8.562	8.588	8.501	3.022	.003	3.330	.001	1.047	.298
	Inf frontoccipital fasc	8.402	8.573	8.601	8.509	3.200	.002	3.323	.001	1.521	.131
	Cingulum	7.747	7.847	7.857	7.823	2.451	.015	2.506	.013	1.316	.191
	Uncinate	8.580	8.716	8.717	8.712	2.913	.004	2.669	.008	2.192	.030
	Middle fronto-orbital	9.614	9.779	9.838	9.639	2.166	.031	2.582	.010	0.242	.809
	Middle frontal WM	8.323	8.408	8.425	8.367	2.580	.010	2.911	.004	0.920	.360
	Inferior frontal WM	8.198	8.281	8.304	8.225	2.157	.032	2.527	.012	0.514	.608
	Middle temporal WM	8.512	8.577	8.599	8.525	1.781	.076	2.236	.026	0.256	.798
	Inferior temporal WM	8.752	8.940	8.934	8.953	3.964	.000	3.432	.001	3.157	.002
Nuc.	Thalamus	8.360	8.505	8.501	8.514	3.065	.002	2.743	.007	2.246	.027
	Putamen	7.184	7.349	7.383	7.271	3.638	.000	3.974	.000	1.432	.155
Resting state fMRI											
	PoCGL_CerebellumL	0.339	0.529	0.565	0.446	4.279	.000	4.364	.000	2.178	.033
	PoCGL_CerebellumR	0.362	0.560	0.603	0.460	4.401	.000	4.575	.000	2.048	.045
	SPGL_ThalamusR	0.102	0.299	0.322	0.245	4.350	.000	4.456	.000	2.119	.040
	SPGR_ThalamusR	0.132	0.309	0.344	0.227	4.092	.000	4.401	.000	1.617	.113
	PrCGL_CerebellumR	0.402	0.588	0.619	0.513	4.188	.000	4.289	.000	2.023	.048
	PrCGL_CerebellumL	0.360	0.541	0.567	0.481	4.131	.000	4.109	.000	2.176	.035
	PrCGL_ThalamusR	0.262	0.449	0.479	0.379	4.014	.000	4.138	.000	1.808	.078
	MTGR_ThalamusR	0.133	0.321	0.361	0.227	3.729	.000	4.121	.000	1.389	.171
	PoCGR_CerebellumR	0.355	0.545	0.565	0.499	4.253	.000	4.051	.000	2.495	.016
	SOGL_CuR	0.916	1.064	1.102	0.975	3.480	.001	4.005	.000	0.976	.334
	IOGR_ThalamusR	0.102	0.282	0.302	0.235	4.042	.000	4.014	.000	2.251	.029
	SPGL_GPR	0.114	0.237	0.273	0.154	3.319	.001	3.958	.000	0.784	.437
	SFGR_SPGL	0.335	0.504	0.523	0.460	3.361	.001	3.463	.001	1.824	.074
	MFOGR_STGR_pole	0.387	0.236	0.236	0.238	-3.914	.000	-3.608	.000	-2.911	.005

TABLE 2 (Continued)

	Group means				HC vs. FEP		HC vs. S-FEP		HC vs. M-FEP	
	HC	FEP	S-FEP	M-FEP	T	p-value	T	p-value	T	p-value
PoCGL_SMGL	0.488	0.675	0.685	0.652	3.775	.000	3.469	.001	2.826	.006
PoCGL_SMGR	0.538	0.680	0.711	0.606	3.107	.002	3.479	.001	1.204	.233
PoCGL_IOGR	0.349	0.530	0.548	0.487	3.526	.001	3.495	.001	2.046	.046
PoCGL_ThalamusR	0.229	0.414	0.439	0.357	3.769	.000	3.824	.000	1.831	.074
PoCGR_PrCGL	1.020	1.193	1.219	1.132	3.292	.001	3.549	.001	1.705	.093
PoCGR_SPGL	0.352	0.590	0.593	0.583	4.057	.000	3.629	.000	3.368	.001
PoCGR_ThalamusL	0.217	0.370	0.399	0.304	3.156	.002	3.500	.001	1.206	.234
PoCGR_ThalamusR	0.252	0.425	0.456	0.354	3.501	.001	3.733	.000	1.472	.148
PrCGL_SPGL	0.435	0.638	0.643	0.627	3.949	.000	3.507	.001	3.127	.003
PrCGL_SPGR	0.447	0.650	0.669	0.605	3.774	.000	3.642	.000	2.680	.009
PrCGL_IOGR	0.337	0.532	0.537	0.520	3.972	.000	3.684	.000	2.628	.012
PrCGL_ThalamusL	0.246	0.417	0.441	0.361	3.601	.000	3.722	.000	1.765	.084
PrCGR_SPGL	0.442	0.651	0.653	0.645	4.003	.000	3.550	.001	3.365	.001
PrCGR_IOGR	0.386	0.559	0.566	0.543	3.787	.000	3.535	.001	2.524	.015
PrCGR_CerebellumL	0.425	0.580	0.606	0.518	3.457	.001	3.545	.001	1.694	.096
PrCGR_CerebellumR	0.376	0.553	0.579	0.492	3.819	.000	3.815	.000	2.154	.035
PrCGR_ThalamusR	0.271	0.450	0.480	0.380	3.568	.000	3.845	.000	1.489	.144
SPGL_ThalamusL	0.124	0.277	0.294	0.236	3.324	.001	3.477	.001	1.654	.105
SPGR_dorsal_ACCL	0.371	0.543	0.589	0.436	3.255	.001	3.732	.000	1.035	.305
SPGR_dorsal_ACCR	0.417	0.570	0.612	0.473	3.156	.002	3.566	.001	0.996	.323
SPGR_CerebellumR	0.370	0.532	0.570	0.444	3.494	.001	3.828	.000	1.446	.153
SPGR_ThalamusL	0.117	0.271	0.301	0.199	3.446	.001	3.769	.000	1.366	.178
SMGL_CerebellumL	0.253	0.409	0.441	0.333	3.505	.001	3.724	.000	1.401	.168
SMGR_ThalamusR	0.163	0.323	0.356	0.246	3.329	.001	3.525	.001	1.492	.141
AGL_PCCR	0.443	0.612	0.609	0.621	3.949	.000	3.486	.001	2.792	.008
STGL_CerebellumL	0.315	0.448	0.491	0.346	2.929	.004	3.514	.001	0.535	.595
STGL_ThalamusR	0.277	0.461	0.493	0.388	3.351	.001	3.530	.001	1.492	.142
STGR_CerebellumL	0.307	0.454	0.489	0.374	3.439	.001	3.816	.000	1.169	.248
STGR_ThalamusR	0.276	0.452	0.488	0.368	3.241	.001	3.587	.000	1.164	.251
MTGL_PCCL	0.522	0.640	0.676	0.556	2.987	.003	3.696	.000	0.567	.573
MTGL_ThalamusL	0.159	0.308	0.342	0.228	3.118	.002	3.569	.001	0.968	.339
MTGL_ThalamusR	0.135	0.286	0.329	0.186	3.045	.003	3.633	.000	0.683	.498
MTGR_PCCL	0.470	0.597	0.621	0.542	3.247	.001	3.496	.001	1.356	.181
MTGR_CerebellumL	0.380	0.504	0.541	0.418	2.967	.004	3.496	.001	0.658	.514
MTGR_PutR	0.127	0.272	0.307	0.188	3.211	.002	3.667	.000	1.068	.290
MTGR_ThalamusL	0.127	0.294	0.327	0.216	3.433	.001	3.739	.000	1.361	.180
FuGL_ThalamusR	0.133	0.275	0.301	0.214	3.250	.001	3.478	.001	1.352	.183
SOGL_ThalamusR	0.121	0.259	0.283	0.203	3.352	.001	3.535	.001	1.464	.150
SOGR_ThalamusR	0.116	0.251	0.268	0.211	3.284	.001	3.501	.001	1.560	.126
MOGL_ThalamusR	0.174	0.318	0.358	0.224	3.287	.001	3.859	.000	0.796	.430
MOGR_ThalamusR	0.156	0.299	0.325	0.236	3.350	.001	3.682	.000	1.260	.215
IOGL_ThalamusR	0.112	0.261	0.284	0.208	3.327	.001	3.472	.001	1.474	.148
IOGR_LGL	0.412	0.614	0.633	0.570	3.614	.000	3.539	.001	2.190	.033
IOGR_CerebellumL	0.450	0.589	0.608	0.545	3.424	.001	3.488	.001	1.781	.081
LGL_CerebellumL	0.471	0.600	0.627	0.537	3.347	.001	3.641	.000	1.344	.185

(Continues)

TABLE 2 (Continued)

	Group means				HC vs. FEP		HC vs. S-FEP		HC vs. M-FEP	
	HC	FEP	S-FEP	M-FEP	T	p-value	T	p-value	T	p-value
LGR_CerebellumL	0.426	0.564	0.587	0.511	3.621	.000	3.745	.000	1.764	.084
LGR_CerebellumR	0.415	0.557	0.575	0.516	3.556	.001	3.553	.001	1.919	.061
LGR_ThalamusR	0.178	0.341	0.345	0.333	3.781	.000	3.491	.001	2.604	.012
SPGR_CerebellumL	0.418	0.562	0.596	0.482	3.105	.002	3.445	.001	1.146	.256
MTGR_CerebellumR	0.375	0.500	0.535	0.419	2.951	.004	3.454	.001	0.737	.465
MTGR_PutL	0.116	0.252	0.281	0.185	3.154	.002	3.448	.001	1.381	.172
PoCGL_SPGL	0.460	0.671	0.679	0.653	3.735	.000	3.418	.001	2.661	.010
PoCGL_SPGR	0.516	0.702	0.724	0.650	3.408	.001	3.417	.001	2.182	.032
IOGR_LGR	0.418	0.617	0.634	0.575	3.511	.001	3.415	.001	2.189	.033
STGR_CerebellumR	0.308	0.446	0.479	0.367	3.067	.003	3.405	.001	1.030	.308
SMGL_CerebellumR	0.286	0.419	0.452	0.341	3.035	.003	3.397	.001	0.983	.330
LGL_CerebellumR	0.444	0.571	0.595	0.515	3.145	.002	3.395	.001	1.344	.185
SPGR_PrCuL	0.418	0.590	0.615	0.532	3.212	.002	3.389	.001	1.626	.110
PoCGL_ThalamusL	0.215	0.373	0.397	0.317	3.184	.002	3.373	.001	1.442	.156
STGL_CerebellumR	0.327	0.452	0.499	0.342	2.716	.007	3.375	.001	0.257	.798
PrCGR_ThalamusL	0.231	0.388	0.413	0.328	3.072	.003	3.327	.001	1.336	.188
SPGL_LGR	0.271	0.451	0.456	0.442	3.663	.000	3.330	.001	2.713	.009
FuGR_ThalamusR	0.132	0.267	0.292	0.209	3.092	.002	3.338	.001	1.295	.201
IOGR_ThalamusL	0.101	0.257	0.266	0.235	3.503	.001	3.336	.001	2.273	.027
PoCGR_SMGL	0.402	0.588	0.592	0.580	3.574	.001	3.314	.001	2.683	.009
PoCGR_CerebellumL	0.402	0.550	0.570	0.505	3.348	.001	3.299	.001	1.740	.089
SPGL_dorsal_ACCL	0.389	0.528	0.567	0.437	2.842	.005	3.284	.001	0.751	.457
SPGL_PCCR	0.154	0.325	0.330	0.314	3.479	.001	3.286	.001	2.182	.035
SPGL_CerebellumR	0.420	0.568	0.593	0.509	3.067	.003	3.274	.001	1.531	.131

Note: For the DTI analysis of FA and MD, the white matter is categorized in projection, association, and commissural (corpus callosum) fibers. We also analyzed deep nuclei and the white matter as a whole ("total white matter"). *p*-value of 0 indicates *p*-value < .0001.

Abbreviations: L: left, R: right; post: posterior, ant: anterior, sup: superior, inf: inferior, int: internal, fasc: fasciculus, WM: white matter. PoCG, PrCG: postcentral, precentral gyrus; SFG: superior frontal; MFOG: middle frontorbital gyrus; SPG: superior parietal gyrus; MTG, STG: middle, inferior temporal gyrus; SOG, IOG, MOG: superior, inferior, middle occipital gyrus; SMG: supramarginal gyrus; AG: angular gyrus; Fu: fusiform gyrus; CU: cuneus gyrus; LG: lingual gyrus; ACC, PCC: anterior, posterior cingulate cortex; GP: globus pallidus; Put: putamen.

fasciculus, and the posterior corona radiate). These common features may suggest a common pathology in FEP. Other features of the latent factors were unique to a single given population (e.g., FA in the uncinate fasciculus, the middle cerebellar peduncle, and the middle and the lateral fronto-orbital areas, were only identified in the S-FEP factor). These specific features may express distinctions among FEP subgroups. Within each group comparison, the SIFA factors showed a large overlap of features between FA and MD. This is consistent with the DTI properties, in which the FA and MD signals go in different directions.

Among all selected features, the thalamus was the structure most consistently identified across all modalities (Figures 2 and 3). Rs-fMRI correlations involving the thalamus and multiple cortical regions, particularly in the temporal areas, were selected in all SIFA factors within all comparisons. Thalamic FA and MD were selected in factors identified in the comparison between FEP versus HC and S-FEP versus HC.

By using the SIFA factors, we accessed the power of features from singular and multiple modalities in order to classify individuals into the FEP group and its subgroups. Considering each singular modality, FA was the most effective modality in classifying the FEP groups vs. the HC group (Table 4). The integration of features from multiple modalities outperformed any singular modality used to classify S-FEP versus HC (Figure 4). The model created with SIFA multimodality factors achieved 77% of correct classification of S-FEP individuals, after cross-validation. Due to the sample size and lack of comparable external dataset for testing, we used leave-one-out cross validation to minimize overfitting.

Using the factors identified by SIFA yielded more robust and better performance compared with the SVM approaches. Table B S2 of the supplementary materials shows the sensitivity, specificity, and F1 score of the classification performance using the latent factors estimated from SIFA. The percentage of variation explained by the common and individual factors, as well as by all latent factors, are presented in Table B S1 of

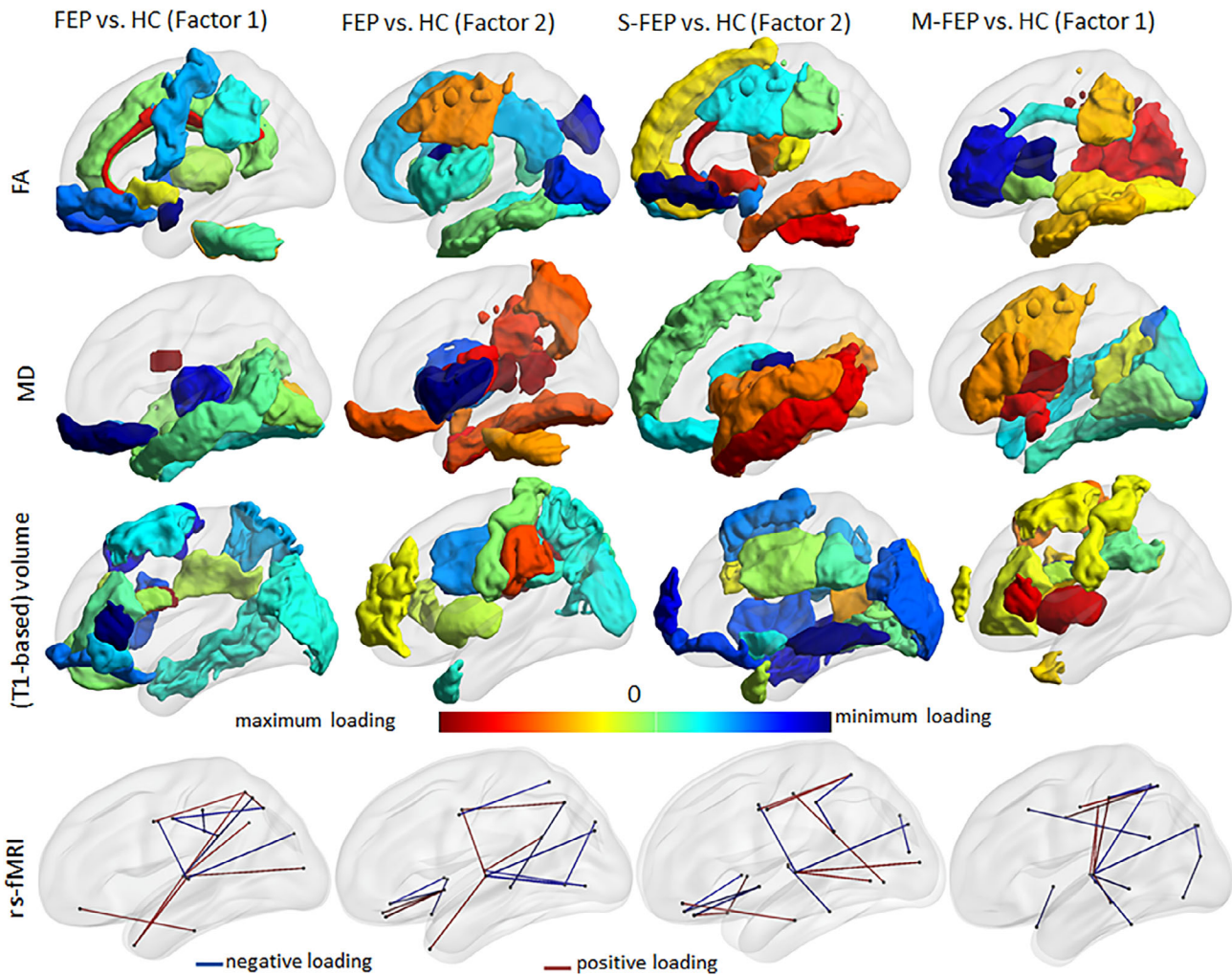


FIGURE 3 Characterization of FEP group and subgroups (S-FEP and M-FEP), compared with controls, by the SIFA. Representation of the regional loadings of the common factors that show significant difference between groups (two in the all FEP vs. HC, one in the S-FEP vs. HC, and one in the M-FEP vs. HC), in a glass brain. The loading values are reported in Table 3. Visualization with the BrainNet Viewer (<http://www.nitrc.org/projects/bnv/>, by Xia et al., 2013)

the supplementary materials. The confidence intervals of the model coefficients presented in Supplementary Figure S1 were obtained following a bootstrap procedure.

4 | DISCUSSION

The goal of this study is to establish a pipeline that allows us to obtain meaningful brain imaging results from a relatively small sample size. We demonstrated a successful case of utilizing an unbiased, data-driven, structure-based analysis to characterize FEP patients. We reduced the dimensionality of the data while still preserving the individual variability, and enhanced the statistical sensitivity and power (Glasser et al., 2016). As an example, with a sample size 50 times smaller than that recently used by the ENIGMA group (27), we were able to detect similar microstructural abnormalities in DTI. The pipeline used here employs “anatomical” filters; that is, the structures in

question. The definition of these structures is based on previous biological knowledge, making the interpretation of the results and possible clinical translation more straightforward (Faria et al., 2017). Using a similar set of labels for multiple modalities facilitates the combination of features derived from these modalities as well as the application of statistical methods for data fusion, such as SIFA. On the other hand, because the structure-based analysis requires spatial predefinitions, it introduces challenges as the choice of parcellation and the level of granularity to be used. For example, if the phenomenon in question spatially mismatches the parcellation scheme employed, it is likely overlooked (Faria et al., 2015), a problem aggravated by the data-driven design. Therefore, the structure-based analysis is a complementary approach, rather than an alternative, to the voxel-based analysis.

In the same way, SIFA is a supervised approach that facilitates the association with auxiliary covariates compared with other methodologies for dimension reduction, such as joint ICA (Moosmann,

TABLE 3 Sparsified loadings of the common factors that show significant difference between groups in the supervised integrated factor analysis (SIFA)

FEP vs. HC	rsfMRI	Loading	FA	Loading	MD	Loading	Volume	Loading
Factor 1 positive	STG R-thalamus R	0.166	GenuCC	0.244	SFO R	0.287	SFO R	0.378
	STG R-thalamus L	0.127	Cingulum R	0.209	IO R	0.142	AntCR R	0.101
	Rectus R-ITG R	0.101	Cingulum L	0.158	SS R	0.084	SLF R	0.097
	MTGpole L-thalamus R	0.063	BodyCC	0.097	IO L	0.063	SFO L	0.082
	Angular R-thalamus R	0.043	MiddleCerebP R	0.095	ST R	0.061	Rectus R	0.064
	MOGL-Thalamus R	0.043	I FO F L	0.06	Uncinate L	0.058	AntCR L	0.034
	SPG R-thalamus R	0.028	Thalamus R	0.035	MT R	0.053		
	SPG R-PrCu L	0.017	Cingulate L	0.022	MT L	0.04		
	SPG R-dorsalACC R	0.014	MiddleCerebP L	0.002	Fusiform R	0.004		
	MTGpole L-thalamus L	0.008						
	PoCG L-SMG R	-0.22	Uncinate L	-0.174	BodyCC	-0.294	IFGtr L	-0.262
	SOG L-thalamus L	-0.071	Uncinate R	-0.144	MFO L	-0.181	SFGR	-0.208
	PrCG R-thalamus L	-0.069	MFO R	-0.099	Thalamus L	-0.127	IFGop R	-0.142
	PrCG L-PrCu L	-0.051	GPR	-0.095	CP L	-0.115	IFGtr R	-0.128
SPG L-thalamus R	-0.035	LFO L	-0.082	Thalamus R	-0.114	LFOG L	-0.108	
PrCG L-SMG L	-0.003	PrC L	-0.062	GenuCC	-0.078	SPG R	-0.069	
		PostCR L	-0.025	SpleniumCC	-0.056	IFGorb L	-0.056	
		PostCR R	-0.001	MFO R	-0.054	SFG L	-0.028	
				CP R	-0.018	MOG L	-0.005	
						MTG R	-0.004	
Factor 2 positive	PCC R-thalamus R	0.031	SupCR R	0.311	RetrolenticularC R	0.114	SMG R	0.275
	MFOG L-insula L	0.027	SupCRL	0.196	SLF R	0.088	SMG L	0.174
	PrCG R-PrCu L	0.022	Insula R	0.095	Putamen L	0.085	MFGdpcf L	0.074
	PrCG R-thalamus L	0.012	IF L	0.09	IT R	0.055	IFGtr R	0.056
	MFOG R-insula L	0.002	PostLimbIC L	0.069	PostLimbIC L	0.049	Put L	0.049
	MTGpole L-thalamus L	0	SLF R	0.068	Fusiform R	0.014	PoCG L	0.024
			IF R	0.061	PrCu R	0.003		
			Insula L	0.051	MFO L	0.002		
			Fusiform L	0.046				
			Caudate R	0.01				
			Cingulate R	0.073				

TABLE 3 (Continued)

	rsfMRI	Loading	FA	Loading	MD	Loading	Volume	Loading
Factor 2 negative	SPG R-dorsalACC L	-0.373	AntLimbIC L	-0.129	Insula L	-0.4	SFO L	-0.102
	STGpole R-put R	-0.215	SpleniumCC	-0.118	Caudate R	-0.303	SupCR L	-0.04
	Lingual R-thalamus L	-0.208	SO R	-0.096	Insula R	-0.27	Cuneus R	-0.034
	SOG R-lingual R	-0.052	IO L	-0.054	MiddleCerebP L	-0.03	PrCu L	-0.028
	IOGR-ThalamusR	-0.035			Total white matter	-0.023	MTGpole L	-0.021
	PrCu L-MTG R	-0.03			Uncinate R	-0.008	PostCR L	-0.01
	LFOGR-InsulaR	-0.03					SOG R	
	LFOGR-InsulaL	-0.018						
	IOGR-ThalamusL	-0.009						
	SOGL-ThalamusL	-0.004						
S-FEP vs. HC	STG pole R-put R	0.163	BodyCC	0.07	SFOFR	0.253	SOG R	0.215
	Rectus R-ITG R	0.154	Cingulum R	0.069	GP R	0.244	Cu R	0.161
	STG R-thalamus R	0.119	Cingulum_L	0.044	MT L	0.195	PTR R	0.111
	SPG R-dorsal ACC L	0.114	MiddleCerebP R	0.04	Insula L	0.107	SOG L	0.089
	SPG R-dorsal ACC R	0.036	IFOF L	0.021	ST L	0.106	SFO L	0.08
	Lingual R-thalamus L	0.028	IFOF R	0.001	MT R	0.105	MFG R	0.075
	MOG L-thalamus L	0.011			ST R	0.087	MTGpole L	0.052
	PoCG R-IOG R	0.009			SS R	0.072	SupCR L	0.042
	MFOG L-STG pole R	0.001					Cu L	0.034
							Lingual L	0.021
Factor 2 negative	MFOG L-insula L	-0.271	LFO L	-0.266	PostLimbIC L	-0.342	SS L	0.014
	FusiformG R-thalamus R	-0.141	LFO R	-0.189	Thalamus L	-0.179	SFG pole L	-0.154
	MFOG R-insula L	-0.137	Uncinate L	-0.181	MFO L	-0.123	MTG R	-0.018
	PrCG R-thalamus L	-0.06	MFO R	-0.157	Caudate L	-0.123	LFOG L	-0.115
	SOG L-thalamus L	-0.058	SupCR L	-0.142	SF L	-0.048	Insula R	-0.087
	MFOG R-insula R	-0.056	PostCR L	-0.098	Putamen L	-0.031	MOG L	-0.083
	PoCG L-SPG R	-0.044	RetrolenticularIC L	-0.056	BodyCC	-0.002	SFGR	-0.076
	SOG R-cu L	-0.031	SF R	-0.05			SMG R	-0.061
	PoCG L-SMG L	-0.022	Rectus R	-0.047	IFG L		IFG L	-0.013
			PostLimbIC L	-0.009	SFG pole R		SFG pole R	-0.011
		Fusiform L	-0.003					

(Continues)

TABLE 3 (Continued)

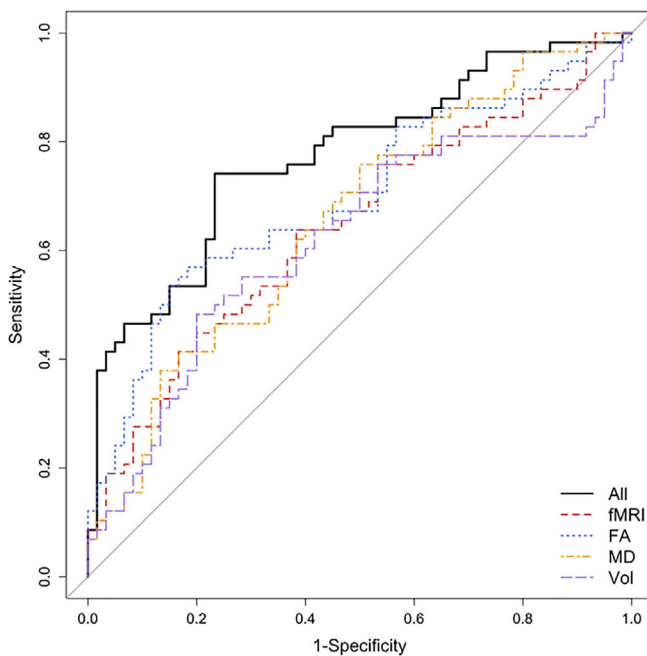
M-FEP vs. HC	Factor 1 positive	rsfMRI	Loading	FA	Loading	MD	Loading	Volume	Loading
		MTG R-thalamus L	0.21	PostCR R	0.145	EC L	0.166	Put R	0.274
		PoCG R-thalamus L	0.078	PostThalamicRad R	0.106	Uncinate L	0.125	IFtr R	0.243
		PrCG L-SPG L	0.051	RetrolenticularIC R	0.105	IFOF L	0.11	Put L	0.217
		PoCG L-thalamus L	0.023	PostCR L	0.049	Putamen L	0.101	IFtr L	0.211
		PrCG R-SPG L	0.014	IF L	0.045	AntLimbIC L	0.074	SFGR	0.1
		PoCG R-thalamus R	0.009	SS L	0.037	InfFrontal L	0.049	Caudate L	0.043
				Fusiform L	0.025	SupCR L	0.035	IFop R	0.038
						GPL	0.002	MTGpole R	0.034
								SFGL	0.005
								BodyCC	0.004
								SFGpole R	0.002
Factor 1 negative		FusiformG R-thalamus R	-0.137	GenuCC	-0.293	IO R	-0.267	SFO R	-0.443
		SPG R-thalamus L	-0.111	AntLimbIC L	-0.17	MO R	-0.173	SLFL	-0.1
		PoCG L-SPG L	-0.101	BodyCC	-0.165	ST R	-0.112	SFO L	-0.044
		IOG R-cu L	-0.085	AntCR L	-0.14	Cuneus R	-0.092	AntCR R	-0.018
		SOG R-cu L	-0.08	AntLimbIC R	-0.064	Fusiform R	-0.082	SLFR	-0.016
		SOG L-thalamus L	-0.079	Cinglum R	-0.047	Lingual R	-0.05	ACR L	-0.012
		MTG L-thalamus R	-0.074	CP R	-0.008	PostThalamicRad R	-0.008	PoCG L	-0.005
		PoCG L-SPG R	-0.069	IFOF L	-0.003				
		MFG R-PCC L	-0.034						
		STG R-thalamus R	-0.034						
		STGpole R-put R	-0.021						

Abbreviations: Cortex*: SFG, MFG, IFG: superior, middle, inferior frontal gyri; IFGtr, IFGop, IFGorb: pars triangularis, opercularis, and orbitalis of IFG; MFGdpcf: dorsal prefrontal cortex; MFOG, LFOG: medium and lateral frontorbital gyri; STG, MTG, ITG: superior, middle, and inferior temporal gyri; SOG, MOG, IOG: superior, middle, and inferior occipital gyri; PrCG, PoCG: pre and post central gyri; PCC, ACC: posterior and anterior cingulate cortex; SMG: supramarginal gyrus; SPG: superior parietal gyrus; PrCu: precuneus gyrus.* For the analysis of FA and MD, the ROIs (no "G") represent the white matter beneath the cortex. Deep white matter: IFOF: inferior frontooccipital fasciculus; ILF, SFL: inferior and superior longitudinal fasciculus; IC: EC: internal and external capsule; CP, CerebP: cerebral and cerebellar peduncle; CC: corpus callosum; CR: corona radiata, SS: sagittal stratum. Put: Putamen, GP: Globus Pallidus. Post, Ant, Sup, Inf: posterior, anterior, superior, inferior; L, R: left, right.

TABLE 4 Area under the curve (95% confidence interval) for the leave-one-out cross-validated receiver-operating characteristic (ROC) curves classifying of FEP and controls

	FEP vs. HC	S-FEP vs. HC	M-FEP vs. HC
All	0.75 (0.67–0.82)	0.77 (0.69–0.86)	0.69 (0.54–0.84)
Rs-fMRI	0.69 (0.6–0.78)	0.64 (0.54–0.74)	0.59 (0.44–0.74)
FA	0.75 (0.67–0.83)	0.7 (0.6–0.79)	0.7 (0.57–0.84)
MD	0.64 (0.55–0.74)	0.66 (0.56–0.76)	0.6 (0.46–0.73)
T1-volume	0.66 (0.57–0.75)	0.62 (0.51–0.72)	0.57 (0.43–0.71)

Note: “All” includes features from all the modalities (T1-based volumes, DTI metrics (fractional anisotropy – FA and mean diffusivity – MD) and resting state fMRI.

**FIGURE 4** Leave-one-out cross-validated ROC curve for the classification of S-FEP and controls. The logistic models were trained using the factors (both common and individual) estimated from the SIFA. The model including multimodality-imaging features (volumes, FA, MD, and rs-fMRI synchrony) was the most effective on correctly classifying individuals with S-FEP, achieving an accuracy of 77% (Table 4)

Eichele, Nordby, Hugdahl, & Calhoun, 2008). A limitation of SIFA is that the estimation procedure was derived from the normal likelihood function, which assumes the data follow Gaussian distributions. Joint ICA was designed for nonnormal data. Therefore, in our study, when implementing SIFA, proper data transformation was done to satisfy the normal assumption, for example, the functional connectivity was Fisher z-transformed. With strong associations between the covariates and the latent structure of the multimodal imaging data, incorporating the supervised effects from covariates improves estimation accuracy and interpretability. By its particular comprehensibility and power, the combination of SIFA with the structure-based approach is particularly relevant for translational studies, hypothesis-generation, and for multimodal characterization of modest samples.

The power of this multimodal characterization is evidenced by the fact that multiple modality classifiers were shown to be more efficient than single modalities in classifying S-FEP individuals. Previous MRI studies applying multivariate machine-learning algorithms in neuroimaging have shown the potential to discriminate between individuals with schizophrenia and HCs (Cabral et al., 2016; Cetin, Houck, Vergara, Miller, & Calhoun, 2015; Du et al., 2012; Lei et al., 2020; Peruzzo, et al., 2015; Qureshi et al., 2017; Sui et al., 2013). The large range of discrimination accuracy previously reported (72–100%) is explained by the variability in samples sizes, differences in the populations and type of images analyzed, differences in validation approaches, and the “publication bias” (only the best performances are published). However, conclusions drawn from patients with established schizophrenia, whose brain structure is known to be affected by the disease chronicity and long term treatment, may not be less robust to FEP individuals. In fact, efficient models to discriminate chronic schizophrenic patients from HCs demonstrate poor generalizability in FEP (de Moura et al., 2018; Pinaya et al., 2016; Vieira et al., 2020). Although multimodal classifiers for FEP are rarely reported, we found that the better performance of our multimodal classifier for S-FEP versus HCs, compared with the single modality classifiers, aligns to what was previously observed in the classification of ultra-high-risk individuals for psychosis, FEP, and HC (Pettersson-Yeo et al., 2014).

In the present study, the accuracy of the classifier was increased by the combination of rs-fMRI abnormalities, which were more specific to the S-FEP group, with more “general” DTI abnormalities, which were greater in the S-FEP group. This points to the value in using multimodal data integration to stratify a heterogeneous population (e.g., FEP) into subgroups of potential clinical relevance. Our group previously reported greater cognitive impairment in individuals with schizophrenia as compared with those with bipolar disorder (Schretlen et al., 2007). Other studies attempted to perform subtype prediction (Arribas, Calhoun, & Adali, 2010; Calhoun, Maciejewski, Pearson, & Kiehl, 2008; Costafreda et al., 2011; Ota et al., 2013; Pardo et al., 2006; Rashid et al., 2016; Sacchet, Livermore, Iglesias, Glover, & Gotlib, 2015; Schnack et al., 2014; Yang et al., 2018; Schretlen et al., 2007 #1853). Although most of these studies used single modality classifiers and focused on different subgroups, they all show predictive value in modeling of “spectrum-like” mental illness. The subgroup distinction supported by SIFA in the present study is in accordance to this notion, and adds proof of the potential value method for stratification in early disease stage.

The comprehensive characterization of the FEP population and its subgroups highlights brain areas that may represent an important locus of the pathology. One of our main findings point to widespread abnormalities in DTI (FA increase and/or MD decrease) in projection and commissural pathways. This was a very robust finding, as diverse anatomically related segments showed the same pattern, agreeing with previous findings of single modality studies in FEP (Cheung et al., 2008; Faria et al., 2019; Lyall et al., 2018; Mitelman et al., 2007; Perez-Iglesias et al., 2010; Price et al., 2007; Schmidt et al., 2015; Wang et al., 2011; Whitford et al., 2010; Zhou et al., 2017) and in data-driven, large sample studies of schizophrenia patients (Kelly et al., 2017; Oestreich et al., 2017). Although stronger in S-FEP, most of the DTI features were shared in S-FEP and M-FEP and suggest involvement with common pathology.

In contrast to the widespread DTI features, within the functional modality we found more localized effects, and the thalamus was among the areas providing the greatest contribution to classification. The particular pattern of connectivity between the thalamus and the somatosensorial cortex we observed in S-FEP aligns with observations in patients with psychotic disorders, individuals at high risk, and those in early and chronic stages of schizophrenia, as well as with reports by our group and others of structural and metabolic abnormalities centered in the thalamus (Agcaoglu et al., 2017; Altamura et al., 2017; Anticevic, 2017; Cho et al., 2016; Cho et al., 2019; Dandash, Pantelis, & Fornito, 2017; Dietsche, Kircher, & Falkenberg, 2017; Gheiratmand et al., 2017; Guo et al., 2015; Li et al., 2017; Merritt, Egerton, Kempton, Taylor, & McGuire, 2016; Murray & Anticevic, 2017; Pinault, 2017; Stephan, Friston, & Frith, 2009; Tu et al., 2019; van Erp et al., 2016; Wang et al., 2019; Woodward & Heckers, 2016; Woodward, Karbasforoushan, & Heckers, 2012; Yaesoubi et al., 2017). Note that thalamus was identified as an important structure for classification "cross-modalities," adding evidences to its core involvement in psychosis.

The connections between thalamus and temporal areas, and among temporal areas and basal frontal areas, were also identified as important features for classification of FEP individuals, in agreement with similar reports in patients with established schizophrenia (Lei et al., 2020). This is physiologically reasonable given the role of these areas for cognitive functions and sensory integration. Although we are tempted to draw direct correlations between brain regions and function, results from multimodal integration must be interpreted as a spatially distributed pattern rather than focusing in individual regions or features. Together, our findings indicate that both functional and physical characteristics (note that volumes of different structures were identified as important features by SIFA, despite of the lack of volumetric group differences) are implicated in FEP at the individual level.

Although our methodology is optimized for relatively modest samples, increasing the cohort would allow us to test the models in independent data, as well as cluster patients into more specific groups. A second limitation is that most of the patients were receiving psychiatric treatment at the time of the scans. The value of these findings must ultimately be proved in drug-naïve cohorts. Information about self-education level, handedness, disease stage, and non-antipsychotic medications was not quantitatively available; these

factors were not included in our analysis. Finally, the DWI was acquired with nonisotropic voxels, which may introduce issues related to partial volume effects. Despite these limitations, it is reasonable to infer that multimodal imaging features carry information about psychosis overall, FEP subgroups and FEP individuals. The present study may serve as a proof-of-concept for the potential of this methodology to be used in the study of a broader range of neurological and psychiatric disorders. The combination of multiple observables within neuroimaging and across nonimage domains is crucial for conditions like FEP and most other psychiatric disorders in which there is no single dominant discriminating feature. In these cases, the subgroup and individual characterization is more likely to reside in multiple features of small effect size that capture different aspects of the condition.

ACKNOWLEDGMENTS

We thank study participants and the recruitment team staff members led by Ms. Yukiko Lema. We thank Ms. Rebecca Schaub for editing the manuscript. This work was supported by NIH (MH-094268, MH-092443, MH-105660, and MH-107730), as well as foundation grants of Stanley, RUSK/S-R, NARSAD/BBRF to AS. A part of the recruitment cost was also supported by Mitsubishi Tanabe Pharma Corporation. This work represents the author's view, independently of the funding sources. The views and opinions expressed in this article are those of the authors and should not be construed as representing the views of the sponsoring organizations, agencies, or U.S. government.

CONFLICT OF INTERESTS

S. Mori and M. I. Miller own "AnatomyWorks". Dr. Mori is its CEO. This arrangement is managed by the Johns Hopkins University in accordance with its conflict-of-interest policies. All the authors have declared no biomedical financial interests or potential conflicts of interest.

AUTHOR CONTRIBUTIONS

Andreia V. Faria: conceived, designed and performed the analysis; contributed analysis tools, wrote the paper. Yi Zhao: performed the analysis, contributed analysis tools, edited the paper. Chenfei Ye, Johnny Hsu: performed the analysis. Elizabeth Cifuentes: collected data. Lei Wang: contributed discussion. Susumu Mori, Michael Miller, Brian Caffo: contributed analysis tools. Akira Sawa: collected data, edited the paper, contributed discussion.

DATA AVAILABILITY STATEMENT

The data analyzed in this study and the analytical code are available under request to the authors.

ORCID

Andreia V. Faria  <https://orcid.org/0000-0002-1673-002X>

Lei Wang  <https://orcid.org/0000-0003-3870-3388>

REFERENCES

- Agcaoglu, O., Miller, R., Damaraju, E., Rashid, B., Bustillo, J., Cetin, M. S., ... Calhoun, V. D. (2017). Decreased hemispheric connectivity and decreased intra- and inter-hemisphere asymmetry of resting state

- functional network connectivity in schizophrenia. *Brain Imaging and Behavior*, 12(3), 615–630.
- Aine, C. J., Bockholt, H. J., Bustillo, J. R., Cañive, J. M., Caprihan, A., Gasparovic, C., ... Calhoun, V. D. (2017). Multimodal neuroimaging in schizophrenia: Description and dissemination. *Neuroinformatics*, 15, 343–364.
- Alonso-Solis, A., Corripio, I., de Castro-Manglano, P., Duran-Sindreu, S., Garcia-Garcia, M., Proal, E., ... Castellanos, F. X. (2012). Altered default network resting state functional connectivity in patients with a first episode of psychosis. *Schizophrenia Research*, 139, 13–18.
- Altamura, A. C., Delvecchio, G., Marotta, G., Oldani, L., Pigoni, A., Ciappolino, V., ... Brambilla, P. (2017). Structural and metabolic differentiation between bipolar disorder with psychosis and substance-induced psychosis: An integrated MRI/PET study. *European Psychiatry: The Journal of the Association of European Psychiatrists*, 41, 85–94.
- Anticevic, A. (2017). Understanding the role of thalamic circuits in schizophrenia neuropathology. *Schizophrenia Research*, 180, 1–3.
- Arbabshirani, M. R., Plis, S., Sui, J., & Calhoun, V. D. (2017). Single subject prediction of brain disorders in neuroimaging: Promises and pitfalls. *NeuroImage*, 145, 137–165.
- Argyelan, M., Gallego, J. A., Robinson, D. G., Ikuta, T., Sarpal, D., John, M., ... Szeszko, P. R. (2015). Abnormal resting state fMRI activity predicts processing speed deficits in first-episode psychosis. *Neuropsychopharmacology: Official Publication of the American College of Neuropsychopharmacology*, 40, 1631–1639.
- Arribas, J. I., Calhoun, V. D., & Adali, T. (2010). Automatic Bayesian classification of healthy controls, bipolar disorder, and schizophrenia using intrinsic connectivity maps from fMRI data. *IEEE Transactions on Bio-Medical Engineering*, 57, 2850–2860.
- Baglivo, V., Cao, B., Mwangi, B., Bellani, M., Perlini, C., Lasalvia, A., ... Brambilla, P. (2018). Hippocampal subfield volumes in patients with first-episode psychosis. *Schizophrenia Bulletin*, 44, 552–559.
- Bang, M., Park, H. J., Pae, C., Park, K., Lee, E., Lee, S. K., & An, S. K. (2018). Aberrant cerebro-cerebellar functional connectivity and minimal self-disturbance in individuals at ultra-high risk for psychosis and with first-episode schizophrenia. *Schizophrenia Research*, 202, 138–140.
- Bassett, D. S., Xia, C. H., & Satterthwaite, T. D. (2018). Understanding the emergence of neuropsychiatric disorders with network neuroscience. *Biological Psychiatry. Cognitive Neuroscience and Neuroimaging*, 3, 742–753.
- Behzadi, Y., Restom, K., Liu, J., & Liu, T. T. (2007). A component based noise correction method (CompCor) for BOLD and perfusion based fMRI. *NeuroImage*, 37, 90–101.
- Benjamini, Y., & Hochberg, Y. (1995). Controlling the false discovery rate: A practical and powerful approach to multiple testing. *Journal of the Royal Statistical Society, Series B*, 57(1), 289–300.
- Breitborde, N. J., Srihari, V. H., & Woods, S. W. (2009). Review of the operational definition for first-episode psychosis. *Early Intervention in Psychiatry*, 3, 259–265.
- Buchy, L., Makowski, C., Malla, A., Joobar, R., & Lepage, M. (2018). A longitudinal study of cognitive insight and cortical thickness in first-episode psychosis. *Schizophrenia Research*, 193, 251–260.
- Cabral, C., Kambeitz-Ilanckovic, L., Kambeitz, J., Calhoun, V. D., Dwyer, D. B., von Saldern, S., ... Koutsouleris, N. (2016). Classifying schizophrenia using multimodal multivariate pattern recognition analysis: Evaluating the impact of individual clinical profiles on the Neurodiagnostic performance. *Schizophrenia Bulletin*, 42(Suppl 1), S110–S117.
- Calhoun, V. D., Maciejewski, P. K., Pearson, G. D., & Kiehl, K. A. (2008). Temporal lobe and "default" hemodynamic brain modes discriminate between schizophrenia and bipolar disorder. *Human Brain Mapping*, 29, 1265–1275.
- Calhoun, V. D., & Sui, J. (2016). Multimodal fusion of brain imaging data: A key to finding the missing link(s) in complex mental illness. *Biological Psychiatry. Cognitive Neuroscience and Neuroimaging*, 1, 230–244.
- Calvo, A., Delvecchio, G., Altamura, A. C., Soares, J. C., & Brambilla, P. (2019). Gray matter differences between affective and non-affective first episode psychosis: A review of Magnetic Resonance Imaging studies: Special Section on "Translational and Neuroscience Studies in Affective Disorders" Section Editor, Maria Nobile MD, PhD. This Section of JAD focuses on the relevance of translational and neuroscience studies in providing a better understanding of the neural basis of affective disorders. The main aim is to briefly summarize relevant research findings in clinical neuroscience with particular regards to specific innovative topics in mood and anxiety disorders. *Journal of Affective Disorders*, 243, 564–574.
- Castro-de-Araujo, L. F. S., & Kanaan, R. A. A. (2017). First episode psychosis moderates the effect of gray matter volume on cognition. *Psychiatry Research: Neuroimaging*, 266, 108–113.
- Cetin, M.S., Houck, J.M., Vergara, V.M., Miller, R.L., Calhoun, V. (2015) Multimodal based classification of schizophrenia patients. Conference proceedings: Annual International Conference of the IEEE Engineering in Medicine and Biology Society. IEEE Engineering in Medicine and Biology Society. Annual Conference, 2015:2629–2632.
- Cheung, V., Cheung, C., McAlonan, G. M., Deng, Y., Wong, J. G., Yip, L., ... Chua, S. E. (2008). A diffusion tensor imaging study of structural dysconnectivity in never-medicated, first-episode schizophrenia. *Psychological Medicine*, 38, 877–885.
- Cho, K. I., Shenton, M. E., Kubicki, M., Jung, W. H., Lee, T. Y., Yun, J. Y., ... Kwon, J. S. (2016). Altered Thalamo-cortical White matter connectivity: Probabilistic tractography study in clinical-high risk for psychosis and first-episode psychosis. *Schizophrenia Bulletin*, 42, 723–731.
- Cho, K. I. K., Kim, M., Yoon, Y. B., Lee, J., Lee, T. Y., & Kwon, J. S. (2019). Disturbed thalamocortical connectivity in unaffected relatives of schizophrenia patients with a high genetic loading. *The Australian and New Zealand Journal of Psychiatry*, 53(9), 889–895.
- Cho, K. I. K., Kwak, Y. B., Hwang, W. J., Lee, J., Kim, M., Lee, T. Y., & Kwon, J. S. (2019). Microstructural changes in higher-order nuclei of the thalamus in patients with first-episode psychosis. *Biological Psychiatry*, 85, 70–78.
- Choe, E., Lee, T. Y., Kim, M., Hur, J. W., Yoon, Y. B., Cho, K. K., & Kwon, J. S. (2018). Aberrant within- and between-network connectivity of the mirror neuron system network and the mentalizing network in first episode psychosis. *Schizophrenia Research*, 199, 243–249.
- Costafreda, S. G., Fu, C. H., Picchioni, M., Touloupoulou, T., McDonald, C., Kravariti, E., ... McGuire, P. K. (2011). Pattern of neural responses to verbal fluency shows diagnostic specificity for schizophrenia and bipolar disorder. *BMC Psychiatry*, 11, 18.
- Dai, Z., Yan, C., Wang, Z., Wang, J., Xia, M., Li, K., & He, Y. (2012). Discriminative analysis of early Alzheimer's disease using multi-modal imaging and multi-level characterization with multi-classifier (M3). *NeuroImage*, 59, 2187–2195.
- Dandash, O., Pantelis, C., & Fornito, A. (2017). Dopamine, fronto-striato-thalamic circuits and risk for psychosis. *Schizophrenia Research*, 180, 48–57.
- de Moura, A. M., Pinaya, W. H. L., Gadelha, A., Zugman, A., Noto, C., Cordeiro, Q., ... Sato, J. R. (2018). Investigating brain structural patterns in first episode psychosis and schizophrenia using MRI and a machine learning approach. *Psychiatry Research: Neuroimaging*, 275, 14–20.
- Deng, Y., Hung, K. S. Y., Lui, S. S. Y., Chui, W. W. H., Lee, J. C. W., Wang, Y., ... Cheung, E. F. C. (2019). Tractography-based classification in distinguishing patients with first-episode schizophrenia from healthy individuals. *Progress in Neuro-Psychopharmacology & Biological Psychiatry*, 88, 66–73.
- Di Biase, M. A., Cropley, V. L., Baune, B. T., Olver, J., Amminger, G. P., Phassouliotis, C., ... Zalesky, A. (2017). White matter connectivity disruptions in early and chronic schizophrenia. *Psychological Medicine*, 47, 2797–2810.
- Dietsche, B., Kircher, T., & Falkenberg, I. (2017). Structural brain changes in schizophrenia at different stages of the illness: A selective review of

- longitudinal magnetic resonance imaging studies. *The Australian and New Zealand Journal of Psychiatry*, 51, 500–508.
- Du, W., Calhoun, V. D., Li, H., Ma, S., Eichele, T., Kiehl, K. A., ... Adali, T. (2012). High classification accuracy for schizophrenia with rest and task fMRI data. *Frontiers in Human Neuroscience*, 6, 145.
- Dukart, J., Smieskova, R., Harrisberger, F., Lenz, C., Schmidt, A., Walter, A., ... Borgwardt, S. (2017). Age-related brain structural alterations as an intermediate phenotype of psychosis. *Journal of Psychiatry & Neuroscience: JPN*, 42, 307–319.
- Dyrba, M., Grothe, M., Kirste, T., & Teipel, S. J. (2015). Multimodal analysis of functional and structural disconnection in Alzheimer's disease using multiple kernel SVM. *Human Brain Mapping*, 36, 2118–2131.
- Emsley, R., Asmal, L., du Plessis, S., Chilliza, B., Phahladira, L., & Kilian, S. (2017). Brain volume changes over the first year of treatment in schizophrenia: Relationships to antipsychotic treatment. *Psychological Medicine*, 47, 2187–2196.
- Faria, A. V., Crawford, J., Ye, C., Hsu, J., Kenkare, A., Schretlen, D., & Sawa, A. (2019). Relationship between neuropsychological behavior and brain white matter in first-episode psychosis. *Schizophrenia Research*, 208, 49–54.
- Faria, A. V., Joel, S. E., Zhang, Y., Oishi, K., van Zijl, P. C., Miller, M. I., ... Mori, S. (2012). Atlas-based analysis of resting-state functional connectivity: Evaluation for reproducibility and multi-modal anatomy-function correlation studies. *NeuroImage*, 61, 613–621.
- Faria, A. V., Liang, Z., Miller, M. I., & Mori, S. (2017). Brain MRI pattern recognition translated to clinical scenarios. *Frontiers in Neuroscience*, 11, 578.
- Faria, A. V., Oishi, K., Yoshida, S., Hillis, A., Miller, M. I., & Mori, S. (2015). Content-based image retrieval for brain MRI: An image-searching engine and population-based analysis to utilize past clinical data for future diagnosis. *NeuroImage: Clinical*, 7, 367–376.
- Fitzsimmons, J., Kubicki, M., & Shenton, M. E. (2013). Review of functional and anatomical brain connectivity findings in schizophrenia. *Current Opinion in Psychiatry*, 26, 172–187.
- Forns-Nadal, M., Berge, D., Sem, F., Mane, A., Igual, L., Guinart, D., & Vilarroya, O. (2017). Increased nucleus accumbens volume in first-episode psychosis. *Psychiatry Research: Neuroimaging*, 263, 57–60.
- Ganella, E. P., Seguin, C., Pantelis, C., Whittle, S., Baune, B. T., Olver, J., ... Bartholomeusz, C. F. (2018). Resting-state functional brain networks in first-episode psychosis: A 12-month follow-up study. *The Australian and New Zealand Journal of Psychiatry*, 52(9), 864–875.
- Gheiratmand, M., Rish, I., Cecchi, G. A., Brown, M. R. G., Greiner, R., Polosecki, P. I., ... Dursun, S. M. (2017). Learning stable and predictive network-based patterns of schizophrenia and its clinical symptoms. *NPJ Schizophrenia*, 3, 22.
- Glasser, M. F., Coalson, T. S., Robinson, E. C., Hacker, C. D., Harwell, J., Yacoub, E., ... Van Essen, D. C. (2016). A multi-modal parcellation of human cerebral cortex. *Nature*, 536, 171–178.
- Gohel, S., Gallego, J. A., Robinson, D. G., DeRosse, P., Biswal, B., & Szeszko, P. R. (2018). Frequency specific resting state functional abnormalities in psychosis. *Human Brain Mapping*, 39, 4509–4518.
- Guma, E., Devenyi, G. A., Malla, A., Shah, J., Chakravarty, M. M., & Pruessner, M. (2017). Neuroanatomical and symptomatic sex differences in individuals at clinical high risk for psychosis. *Frontiers in Psychiatry*, 8, 291.
- Guo, W., Liu, F., Liu, J., Yu, L., Zhang, J., Zhang, Z., ... Zhao, J. (2015). Abnormal causal connectivity by structural deficits in first-episode, drug-naive schizophrenia at rest. *Schizophrenia Bulletin*, 41, 57–65.
- Hirjak, D., Rashidi, M., Fritze, S., Bertolino, A. L., Geiger, L. S., Zang, Z., ... Wolf, R. C. (2019). Patterns of co-altered brain structure and function underlying neurological soft signs in schizophrenia spectrum disorders. *Human Brain Mapping*, 40, 5029–5041.
- Huang, H., Botao, Z., Jiang, Y., Tang, Y., Zhang, T., Tang, X., ... Wang, J. (2020). Aberrant resting-state functional connectivity of salience network in first-episode schizophrenia. *Brain Imaging and Behavior*, 14(5): 1350–1360.
- Huttlova, J., Kikinis, Z., Kerkovsky, M., Bouix, S., Vu, M. A., Makris, N., ... Kasperek, T. (2014). Abnormalities in myelination of the superior cerebellar peduncle in patients with schizophrenia and deficits in movement sequencing. *Cerebellum*, 13, 415–424.
- Jiang, H., van Zijl, P. C., Kim, J., Pearlson, G. D., & Mori, S. (2006). DtiStudio: Resource program for diffusion tensor computation and fiber bundle tracking. *Computer Methods and Programs in Biomedicine*, 81, 106–116.
- Kamath, V., Crawford, J., DuBois, S., Nucifora, F. C., Nestadt, G., Sawa, A., & Schretlen, D. (2019). Contributions of olfactory and neuropsychological assessment to the diagnosis of first-episode schizophrenia. *Neuropsychology*, 33, 203–211.
- Kamath, V., Lasutschinkow, P., Ishizuka, K., & Sawa, A. (2018). Olfactory functioning in first-episode psychosis. *Schizophrenia Bulletin*, 44, 672–680.
- Karlsgodt, K. H., Sun, D., & Cannon, T. D. (2010). Structural and functional brain abnormalities in schizophrenia. *Current Directions in Psychological Science*, 19, 226–231.
- Kasai, K., Shenton, M. E., Salisbury, D. F., Hirayasu, Y., Onitsuka, T., Spencer, M. H., ... McCarley, R. W. (2003). Progressive decrease of left Heschl gyrus and planum temporale gray matter volume in first-episode schizophrenia: A longitudinal magnetic resonance imaging study. *Archives of General Psychiatry*, 60, 766–775.
- Kelly, S., Jahanshad, N., Zalesky, A., Kochunov, P., Agartz, I., Alloza, C., ... Donohoe, G. (2017). Widespread white matter microstructural differences in schizophrenia across 4322 individuals: Results from the ENIGMA schizophrenia DTI working group. *Molecular Psychiatry*, 23(5), 1261–1269.
- Keymer-Gausset, A., Alonso-Solis, A., Corripio, I., Sauras-Quetcuti, R. B., Pomarol-Clotet, E., Canales-Rodríguez, E. J., ... Portella, M. J. (2018). Gray and white matter changes and their relation to illness trajectory in first episode psychosis. *European Neuropsychopharmacology: The Journal of the European College of Neuropsychopharmacology*, 28, 392–400.
- Kim, M.-J., Min, S.-H., & Han, I. (2006). An evolutionary approach to the combination of multiple classifiers to predict a stock price index. *Expert Systems with Applications*, 31, 241–247.
- Kong, X., Ouyang, X., Tao, H., Liu, H., Li, L., Zhao, J., ... Liu, Z. (2011). Complementary diffusion tensor imaging study of the corpus callosum in patients with first-episode and chronic schizophrenia. *Journal of Psychiatry & Neuroscience*, 36, 120–125.
- Kourou, K., Exarchos, T. P., Exarchos, K. P., Karamouzis, M. V., & Fotiadis, D. I. (2015). Machine learning applications in cancer prognosis and prediction. *Computational and Structural Biotechnology Journal*, 13, 8–17.
- Kuang, C., Buchy, L., Barbato, M., Makowski, C., MacMaster, F. P., Bray, S., ... Addington, J. (2017). A pilot study of cognitive insight and structural covariance in first-episode psychosis. *Schizophrenia Research*, 179, 91–96.
- Kuswanto, C. N., Teh, I., Lee, T. S., & Sim, K. (2012). Diffusion tensor imaging findings of white matter changes in first episode schizophrenia: A systematic review. *Clin Psychopharmacol Neurosci*, 10, 13–24.
- Lang, D. J., Khorram, B., Goghari, V. M., Kopala, L. C., Vandorpe, R. A., Rui, Q., ... Honer, W. G. (2006). Reduced anterior internal capsule and thalamic volumes in first-episode psychosis. *Schizophrenia Research*, 87, 89–99.
- Lee, D. Y., Smith, G. N., Su, W., Honer, W. G., Macewan, G. W., Lapointe, J. S., ... Lang, D. J. (2012). White matter tract abnormalities in first-episode psychosis. *Schizophrenia Research*, 141, 29–34.
- Lee, S. H., Niznikiewicz, M., Asami, T., Otsuka, T., Salisbury, D. F., Shenton, M. E., & McCarley, R. W. (2016). Initial and progressive gray matter abnormalities in insular gyrus and temporal pole in first-episode schizophrenia contrasted with first-episode affective psychosis. *Schizophrenia Bulletin*, 42, 790–801.
- Lei, D., Pinaya, W. H. L., Young, J., van Amelsvoort, T., Marcelis, M., Donohoe, G., ... Mechelli, A. (2020). Integrating machine learning and

- multimodal neuroimaging to detect schizophrenia at the level of the individual. *Human Brain Mapping*, 41, 1119–1135.
- Lei, W., Li, N., Deng, W., Li, M., Huang, C., Ma, X., ... Li, T. (2015). White matter alterations in first episode treatment-naive patients with deficit schizophrenia: A combined VBM and DTI study. *Scientific Reports*, 5, 12994.
- Lerman-Sinkoff, D. B., Kandala, S., Calhoun, V. D., Barch, D. M., & Mamah, D. T. (2019). Transdiagnostic multimodal neuroimaging in psychosis: Structural, resting-state, and task magnetic resonance imaging correlates of cognitive control. *Biological Psychiatry. Cognitive Neuroscience and Neuroimaging*, 4, 870–880.
- Lessmann, S., Baesens, B., Seow, H.-V., & Thomas, L. C. (2015). Benchmarking state-of-the-art classification algorithms for credit scoring: An update of research. *European Journal of Operational Research*, 247, 124–136.
- Levin-Schwartz, Y., Calhoun, V. D., & Adali, T. (2017). Quantifying the interaction and contribution of multiple datasets in fusion: Application to the detection of schizophrenia. *IEEE Transactions on Medical Imaging*, 36, 1385–1395.
- Li, G., & Jung, S. (2017). Incorporating covariates into integrated factor analysis of multi-view data. *Biometrics*, 73, 1433–1442.
- Li, T., Wang, Q., Zhang, J., Rolls, E. T., Yang, W., Palaniyappan, L., ... Feng, J. (2017). Brain-wide analysis of functional connectivity in first-episode and chronic stages of schizophrenia. *Schizophrenia Bulletin*, 43, 436–448.
- Lian, N., Lv, H., Guo, W., Shen, Y., Wu, R., Liu, Y., ... Zhao, J. (2018). A comparative study of magnetic resonance imaging on the gray matter and resting-state function in prodromal and first-episode schizophrenia. *American journal of medical genetics. Part B, Neuropsychiatric Genetics: The Official Publication of the International Society of Psychiatric Genetics*, 177, 537–545.
- Long, D., Wang, J., Xuan, M., Gu, Q., Xu, X., Kong, D., & Zhang, M. (2012). Automatic classification of early Parkinson's disease with multi-modal MR imaging. *PLoS One*, 7, e47714.
- Lottman, K. K., White, D. M., Kraguljac, N. V., Reid, M. A., Calhoun, V. D., Catao, F., & Lahti, A. C. (2018). Four-way multimodal fusion of 7 T imaging data using an mCCA+jICA model in first-episode schizophrenia. *Human Brain Mapping*, 39, 1475–1488.
- Lyall, A. E., Pasternak, O., Robinson, D. G., Newell, D., Trampush, J. W., Gallego, J. A., ... Szeszko, P. R. (2018). Greater extracellular free-water in first-episode psychosis predicts better neurocognitive functioning. *Molecular Psychiatry*, 23, 701–707.
- Makowski, C., Lewis, J. D., Lepage, C., Malla, A. K., Joobar, R., Lepage, M., & Evans, A. C. (2019). Structural associations of cortical contrast and thickness in first episode psychosis. *Cerebral cortex (New York, N.Y.: 1991)*, 29(12), 5009–5021.
- McHugo, M., Talati, P., Woodward, N. D., Armstrong, K., Blackford, J. U., & Heckers, S. (2018). Regionally specific volume deficits along the hippocampal long axis in early and chronic psychosis. *NeuroImage. Clinical*, 20, 1106–1114.
- McKeown, M. J., & Sejnowski, T. J. (1998). Independent component analysis of fMRI data: Examining the assumptions. *Human Brain Mapping*, 6, 368–372.
- McNabb, C. B., Tait, R. J., Mclwain, M. E., Anderson, V. M., Suckling, J., Kydd, R. R., & Russell, B. R. (2018). Functional network dysconnectivity as a biomarker of treatment resistance in schizophrenia. *Schizophrenia Research*, 195, 160–167.
- Meng, X., Jiang, R., Lin, D., Bustillo, J., Jones, T., Chen, J., ... Calhoun, V. D. (2017). Predicting individualized clinical measures by a generalized prediction framework and multimodal fusion of MRI data. *NeuroImage*, 145, 218–229.
- Merritt, K., Egerton, A., Kempton, M. J., Taylor, M. J., & McGuire, P. K. (2016). Nature of glutamate alterations in schizophrenia: A meta-analysis of proton magnetic resonance spectroscopy studies. *JAMA Psychiatry*, 73, 665–674.
- Miller, M. I., Faria, A. V., Oishi, K., & Mori, S. (2013). High-throughput neuro-imaging informatics. *Frontiers in Neuroinformatics*, 7, 31.
- Miller, R. L., Vergara, V. M., & Calhoun, V. D. (2018). Detection of relationships among multi-modal brain imaging meta-features via information flow. *Journal of Neuroscience Methods*, 294, 72–80.
- Mitelman, S. A., Torosjan, Y., Newmark, R. E., Schneiderman, J. S., Chu, K. W., Brickman, A. M., ... Buchsbaum, M. S. (2007). Internal capsule, corpus callosum and long associative fibers in good and poor outcome schizophrenia: A diffusion tensor imaging survey. *Schizophrenia Research*, 92, 211–224.
- Moosmann, M., Eichele, T., Nordby, H., Hugdahl, K., & Calhoun, V. D. (2008). Joint independent component analysis for simultaneous EEG-fMRI: Principle and simulation. *International Journal of Psychophysiology: Official Journal of the International Organization of Psychophysiology*, 67, 212–221.
- Mori, S., Oishi, K., Faria, A. V., & Miller, M. I. (2013). Atlas-based neuroinformatics via MRI: Harnessing information from past clinical cases and quantitative image analysis for patient care. *Annual Review of Biomedical Engineering*, 15, 71–92.
- Mori, S., Wu, D., Ceritoglu, C., Li, Y., Kolasny, A., Vaillant, M. A., ... Miller, M. I. (2016). MRICloud: Delivering high-throughput MRI Neuroinformatics as cloud-based software as a service. *Computing in Science & Engineering*, 18, 21–35.
- Moser, D. A., Doucet, G. E., Lee, W. H., Rasgon, A., Krinsky, H., Leibu, E., ... Frangou, S. (2018). Multivariate associations among behavioral, clinical, and multimodal imaging phenotypes in patients with psychosis. *JAMA Psychiatry*, 75, 386–395.
- Murray, J. D., & Anticevic, A. (2017). Toward understanding thalamocortical dysfunction in schizophrenia through computational models of neural circuit dynamics. *Schizophrenia Research*, 180, 70–77.
- Nakamura, M., Salisbury, D. F., Hirayasu, Y., Bouix, S., Pohl, K. M., Yoshida, T., ... McCarley, R. W. (2007). Neocortical gray matter volume in first-episode schizophrenia and first-episode affective psychosis: A cross-sectional and longitudinal MRI study. *Biological Psychiatry*, 62, 773–783.
- Oestreich, L. K., Lyall, A. E., Pasternak, O., Kikinis, Z., Newell, D. T., Savadjiev, P., ... McCarthy-Jones, S. (2017). Characterizing white matter changes in chronic schizophrenia: A free-water imaging multi-site study. *Schizophrenia Research*, 189, 153–161.
- Ota, M., Ishikawa, M., Sato, N., Hori, H., Sasayama, D., Hattori, K., ... Kunugi, H. (2013). Discrimination between schizophrenia and major depressive disorder by magnetic resonance imaging of the female brain. *Journal of Psychiatric Research*, 47, 1383–1388.
- Pagel, T., Baldessarini, R. J., Franklin, J., & Baethge, C. (2013). Characteristics of patients diagnosed with schizoaffective disorder compared with schizophrenia and bipolar disorder. *Bipolar Disorders*, 15, 229–239.
- Pardo, P. J., Georgopoulos, A. P., Kenny, J. T., Stuve, T. A., Findling, R. L., & Schulz, S. C. (2006). Classification of adolescent psychotic disorders using linear discriminant analysis. *Schizophrenia Research*, 87, 297–306.
- Parellada, M., Pina-Camacho, L., Moreno, C., Aleman, Y., Krebs, M. O., Desco, M., ... Janssen, J. (2017). Insular pathology in young people with high-functioning autism and first-episode psychosis. *Psychological Medicine*, 47, 2472–2482.
- Perez-Iglesias, R., Tordesillas-Gutierrez, D., Barker, G. J., McGuire, P. K., Roiz-Santianez, R., Mata, I., ... Crespo-Facorro, B. (2010). White matter defects in first episode psychosis patients: A voxelwise analysis of diffusion tensor imaging. *NeuroImage*, 49, 199–204.
- Peruzzo, D., Castellani, U., Perlini, C., Bellani, M., Marinelli, V., Rambaldelli, G., ... Group, P.I.-V. (2015). Classification of first-episode psychosis: A multimodal multi-feature approach integrating structural and diffusion imaging. *Journal of Neural Transmission (Vienna)*, 122, 897–905.
- Peters, B. D., de Haan, L., Dekker, N., Blaas, J., Becker, H. E., Dingemans, P. M., ... Linszen, D. H. (2008). White matter fibertracking in first-episode schizophrenia, schizoaffective patients and subjects at ultra-high risk of psychosis. *Neuropsychobiology*, 58, 19–28.

- Pettersson-Yeo, W., Benetti, S., Marquand, A. F., Jules, R., Catani, M., Williams, S. C., ... Mechelli, A. (2014). An empirical comparison of different approaches for combining multimodal neuroimaging data with support vector machine. *Frontiers in Neuroscience*, *8*, 189.
- Pinault, D. (2017). A neurophysiological perspective on a preventive treatment against schizophrenia using transcranial electric stimulation of the Corticothalamic pathway. *Brain Sciences*, *7*(4), 34.
- Pinaya, W. H., Gadelha, A., Doyle, O. M., Noto, C., Zugman, A., Cordeiro, Q., ... Sato, J. R. (2016). Using deep belief network modelling to characterize differences in brain morphometry in schizophrenia. *Scientific Reports*, *6*, 38897.
- Power, J. D., Barnes, K. A., Snyder, A. Z., Schlaggar, B. L., & Petersen, S. E. (2012). Spurious but systematic correlations in functional connectivity MRI networks arise from subject motion. *NeuroImage*, *59*, 2142–2154.
- Price, G., Cercignani, M., Parker, G. J., Altmann, D. R., Barnes, T. R., Barker, G. J., ... Ron, M. A. (2007). Abnormal brain connectivity in first-episode psychosis: A diffusion MRI tractography study of the corpus callosum. *NeuroImage*, *35*, 458–466.
- Qi, S., Sui, J., Chen, J., Liu, J., Jiang, R., Silva, R., ... Calhoun, V. D. (2019). Parallel group ICA+ICA: Joint estimation of linked functional network variability and structural covariation with application to schizophrenia. *Human Brain Mapping*, *40*, 3795–3809.
- Qureshi, M. N. I., Oh, J., Cho, D., Jo, H. J., & Lee, B. (2017). Multimodal discrimination of schizophrenia using hybrid weighted feature concatenation of brain functional connectivity and anatomical features with an extreme learning machine. *Frontiers in Neuroinformatics*, *11*, 59.
- Rashid, B., Arbabshirani, M. R., Damaraju, E., Cetin, M. S., Miller, R., Pearlson, G. D., & Calhoun, V. D. (2016). Classification of schizophrenia and bipolar patients using static and dynamic resting-state fMRI brain connectivity. *NeuroImage*, *134*, 645–657.
- Rashid, B., & Calhoun, V. (2020). Towards a brain-based predictive of mental illness. *Human Brain Mapping*, *41*, 3468–3535.
- Ren, H. Y., Wang, Q., Lei, W., Zhang, C. C., Li, Y. F., Li, X. J., ... Li, T. (2017). The common variants implicated in microstructural abnormality of first episode and drug-naive patients with schizophrenia. *Scientific Reports*, *7*, 11750.
- Rezende, T. J. R., Campos, B. M., Hsu, J., Li, Y., Ceritoglu, C., Kuttan, K., ... Faria, A. V. (2019). Test-retest reproducibility of a multi-atlas automated segmentation tool on multimodality brain MRI. *Brain and Behavior: A Cognitive Neuroscience Perspective*, *9*, e01363.
- Rink, L., Pagel, T., Franklin, J., & Baethge, C. (2016). Characteristics and heterogeneity of schizoaffective disorder compared with unipolar depression and schizophrenia - a systematic literature review and meta-analysis. *Journal of Affective Disorders*, *191*, 8–14.
- Rosa, P. G., Zanetti, M. V., Duran, F. L., Santos, L. C., Menezes, P. R., Sczufca, M., ... Schaufelberger, M. S. (2015). What determines continuing grey matter changes in first-episode schizophrenia and affective psychosis? *Psychological Medicine*, *45*, 817–828.
- Sacchet, M. D., Livermore, E. E., Iglesias, J. E., Glover, G. H., & Gotlib, I. H. (2015). Subcortical volumes differentiate major depressive disorder, bipolar disorder, and remitted major depressive disorder. *Journal of Psychiatric Research*, *68*, 91–98.
- Sauras, R., Keymer, A., Alonso-Solis, A., Diaz, A., Molins, C., Nunez, F., ... Corripio, I. (2017). Volumetric and morphological characteristics of the hippocampus are associated with progression to schizophrenia in patients with first-episode psychosis. *European Psychiatry: The Journal of the Association of European Psychiatrists*, *45*, 1–5.
- Schmidt, A., Lenz, C., Smieskova, R., Harrisberger, F., Walter, A., Riecher-Rössler, A., ... Borgwardt, S. J. (2015). Brain diffusion changes in emerging psychosis and the impact of state-dependent psychopathology. *Neuro-Signals*, *23*, 71–83.
- Schnack, H. G., Nieuwenhuis, M., van Haren, N. E., Abramovic, L., Scheewe, T. W., Brouwer, R. M., ... Kahn, R. S. (2014). Can structural MRI aid in clinical classification? A machine learning study in two independent samples of patients with schizophrenia, bipolar disorder and healthy subjects. *NeuroImage*, *84*, 299–306.
- Schretlen, D. J., Cascella, N. G., Meyer, S. M., Kingery, L. R., Testa, S. M., Munro, C. A., ... Pearlson, G. D. (2007). Neuropsychological functioning in bipolar disorder and schizophrenia. *Biological Psychiatry*, *62*, 179–186.
- Schubert, K. O., Clark, S. R., & Baune, B. T. (2015). The use of clinical and biological characteristics to predict outcome following first episode psychosis. *The Australian and New Zealand Journal of Psychiatry*, *49*, 24–35.
- Schultz, C. C., Fusar-Poli, P., Wagner, G., Koch, K., Schachtzabel, C., Gruber, O., ... Schlösser, R. G. (2012). Multimodal functional and structural imaging investigations in psychosis research. *European Archives of Psychiatry and Clinical Neuroscience*, *262*(Suppl 2), S97–S106.
- Serpa, M. H., Doshi, J., Erus, G., Chaim-Avancini, T. M., Cavallet, M., van de Bilt, M. T., ... Zanetti, M. V. (2017). State-dependent microstructural white matter changes in drug-naive patients with first-episode psychosis. *Psychological Medicine*, *47*, 2613–2627.
- Shile, Q., Calhoun, V. D., van Erp, T. G., Damaraju, E., Bustillo, J., Yuhui, D., Turner, J. A., Mathalon, D. H., Ford, J. M., Voyvodic, J., Mueller, B. A., Belger, A., McEwen, S., Potkin, S. G., Preda, A., Birn, F., Tianzi, J., Jing, S. (2016). Supervised multimodal fusion and its application in searching joint neuromarkers of working memory deficits in schizophrenia. Conference proceedings: Annual International Conference of the IEEE Engineering in Medicine and Biology Society. IEEE Engineering in Medicine and Biology Society. Annual Conference, 2016: 4021–4026.
- Stephan, K. E., Friston, K. J., & Frith, C. D. (2009). Dysconnection in schizophrenia: From abnormal synaptic plasticity to failures of self-monitoring. *Schizophrenia Bulletin*, *35*, 509–527.
- Sui, J., Adali, T., Yu, Q., Chen, J., & Calhoun, V. D. (2012). A review of multivariate methods for multimodal fusion of brain imaging data. *Journal of Neuroscience Methods*, *204*, 68–81.
- Sui, J., He, H., Yu, Q., Chen, J., Rogers, J., Pearlson, G. D., ... Calhoun, V. D. (2013). Combination of resting state fMRI, DTI, and sMRI data to discriminate schizophrenia by N-way MCCA + jICA. *Frontiers in Human Neuroscience*, *7*, 235.
- Sui, J., Huster, R., Yu, Q., Segall, J. M., & Calhoun, V. D. (2014). Function-structure associations of the brain: Evidence from multimodal connectivity and covariance studies. *NeuroImage*, *102*(Pt 1), 11–23.
- Tang, X., Oishi, K., Faria, A. V., Hillis, A. E., Albert, M. S., Mori, S., & Miller, M. I. (2013). Bayesian parameter estimation and segmentation in the multi-atlas random orbit model. *PLoS One*, *8*, e65591.
- Tang, X., Yoshida, S., Hsu, J., Huisman, T. A., Faria, A. V., Oishi, K., ... Mori, S. (2014). Multi-contrast multi-atlas parcellation of diffusion tensor imaging of the human brain. *PLoS One*, *9*, e96985.
- Tang, Y., Zhou, Q., Chang, M., Chekroud, A., Gueorguieva, R., Jiang, X., ... Driesen, N. R. (2019). Altered functional connectivity and low-frequency signal fluctuations in early psychosis and genetic high risk. *Schizophrenia Research*, *210*, 172–179.
- Thompson, P. M., Jahanshad, N., Ching, C. R. K., Salminen, L. E., Thomopoulos, S. I., Bright, J., ... Zelman, V. (2020). ENIGMA and global neuroscience: A decade of large-scale studies of the brain in health and disease across more than 40 countries. *Translational Psychiatry*, *10*, 100.
- Tognin, S., van Hell, H. H., Merritt, K., Winter-van Rossum, I., Bossong, M. G., Kempton, M. J., ... McGuire, P. (2020). Towards precision medicine in psychosis: Benefits and challenges of multimodal multicenter studies-PSYSCAN: Translating neuroimaging findings from research into clinical practice. *Schizophrenia Bulletin*, *46*, 432–441.
- Tordesillas-Gutierrez, D., Ayasa-Arriola, R., Delgado-Alvarado, M., Robinson, J. L., Lopez-Morinigo, J., Pujol, J., ... Crespo-Facorro, B. (2018). The right occipital lobe and poor insight in first-episode psychosis. *PLoS One*, *13*, e0197715.

- Tu, P. C., Bai, Y. M., Li, C. T., Chen, M. H., Lin, W. C., Chang, W. C., & Su, T. P. (2019). Identification of common thalamocortical dysconnectivity in four major psychiatric disorders. *Schizophrenia Bulletin*, 45, 1143–1151.
- Ublinski, M. V., Semenova, N. A., Lukovkina, O. V., Sidorin, S. V., Lebedeva, I. S., Kaleda, V. G., ... Akhadov, T. A. (2015). Characteristics of diffusion in the corticospinal tract of patients with early stage of schizophrenia: Diffusion tensor magnetic resonance imaging. *Bulletin of Experimental Biology and Medicine*, 159, 29–31.
- van Erp, T. G., Hibar, D. P., Rasmussen, J. M., Glahn, D. C., Pearlson, G. D., Andreassen, O. A., ... Turner, J. A. (2016). Subcortical brain volume abnormalities in 2028 individuals with schizophrenia and 2540 healthy controls via the ENIGMA consortium. *Molecular Psychiatry*, 21, 547–553.
- Vargas, T., Dean, D. J., Osborne, K. J., Gupta, T., Ristanovic, I., Ozturk, S., ... Mittal, V. A. (2018). Hippocampal subregions across the psychosis Spectrum. *Schizophrenia Bulletin*, 44, 1091–1099.
- Vieira, S., Gong, Q. Y., Pinaya, W. H. L., Scarpazza, C., Tognin, S., Crespo-Facorro, B., ... Mechelli, A. (2020). Using machine learning and structural neuroimaging to detect first episode psychosis: Reconsidering the evidence. *Schizophrenia Bulletin*, 46, 17–26.
- Vita, A., De Peri, L., Deste, G., Barlati, S., & Sacchetti, E. (2015). The effect of antipsychotic treatment on cortical gray matter changes in schizophrenia: Does the class matter? A meta-analysis and meta-regression of longitudinal magnetic resonance imaging studies. *Biological Psychiatry*, 78, 403–412.
- Wang, A. M., Pradhan, S., Coughlin, J. M., Trivedi, A., DuBois, S. L., Crawford, J. L., ... Barker, P. B. (2019). Assessing brain metabolism with 7-T proton magnetic resonance spectroscopy in patients with first-episode psychosis. *JAMA Psychiatry*, 76, 314–323.
- Wang, Q., Deng, W., Huang, C., Li, M., Ma, X., Wang, Y., ... Li, T. (2011). Abnormalities in connectivity of white-matter tracts in patients with familial and non-familial schizophrenia. *Psychological Medicine*, 41, 1691–1700.
- Wang, Z., Meda, S. A., Keshavan, M. S., Tamminga, C. A., Sweeney, J. A., Clementz, B. A., ... Pearlson, G. D. (2015). Large-scale fusion of gray matter and resting-state functional MRI reveals common and distinct biological markers across the psychosis Spectrum in the B-SNIP cohort. *Frontiers in Psychiatry*, 6, 174.
- Whitford, T. J., Kubicki, M., Schneiderman, J. S., O'Donnell, L. J., King, R., Alvarado, J. L., ... Shenton, M. E. (2010). Corpus callosum abnormalities and their association with psychotic symptoms in patients with schizophrenia. *Biological Psychiatry*, 68, 70–77.
- Woodward, N. D., & Heckers, S. (2016). Mapping Thalamocortical functional connectivity in chronic and early stages of psychotic disorders. *Biological Psychiatry*, 79, 1016–1025.
- Woodward, N. D., Karbasforoushan, H., & Heckers, S. (2012). Thalamocortical dysconnectivity in schizophrenia. *The American Journal of Psychiatry*, 169, 1092–1099.
- Xia, C. H., Ma, Z., Ciric, R., Gu, S., Betzel, R. F., Kaczkurkin, A. N., ... Satterthwaite, T. D. (2018). Linked dimensions of psychopathology and connectivity in functional brain networks. *Nature Communications*, 9, 3003.
- Xia, M., Wang, J., & He, Y. (2013). BrainNet viewer: A network visualization tool for human brain connectomics. *PLoS ONE*, 8, e68910.
- Yaesoubi, M., Miller, R. L., Bustillo, J., Lim, K. O., Vaidya, J., & Calhoun, V. D. (2017). A joint time-frequency analysis of resting-state functional connectivity reveals novel patterns of connectivity shared between or unique to schizophrenia patients and healthy controls. *NeuroImage. Clinical*, 15, 761–768.
- Yang, H., Liu, J., Sui, J., Pearlson, G., & Calhoun, V. D. (2010). A hybrid machine learning method for fusing fMRI and genetic data: Combining both improves classification of schizophrenia. *Frontiers in Human Neuroscience*, 4, 192.
- Yang, J., Zhang, M., Ahn, H., Zhang, Q., Jin, T. B., Li, I., ... DeLorenzo, C. (2018). Development and evaluation of a multimodal marker of major depressive disorder. *Human Brain Mapping*, 39, 4420–4439.
- Zhang, D., Wang, Y., Zhou, L., Yuan, H., & Shen, D. (2011). Multimodal classification of Alzheimer's disease and mild cognitive impairment. *NeuroImage*, 55, 856–867.
- Zhao, C., Zhu, J., Liu, X., Pu, C., Lai, Y., Chen, L., ... Hong, N. (2018). Structural and functional brain abnormalities in schizophrenia: A cross-sectional study at different stages of the disease. *Progress in Neuro-Psychopharmacology & Biological Psychiatry*, 83, 27–32.
- Zhou, Y., Liu, J., Driesen, N., Womer, F., Chen, K., Wang, Y., ... Wang, F. (2017). White matter integrity in genetic high-risk individuals and first-episode schizophrenia patients: Similarities and disassociations. *BioMed Research International*, 2017, 3107845.
- Zou, H., Hastie, T., & Tibshirani, R. (2006). Sparse principal component analysis. *Journal of Computational and Graphical Statistics*, 15, 265–286.

SUPPORTING INFORMATION

Additional supporting information may be found online in the Supporting Information section at the end of this article.

How to cite this article: Faria AV, Zhao Y, Ye C, et al.

Multimodal MRI assessment for first episode psychosis: A major change in the thalamus and an efficient stratification of a subgroup. *Hum Brain Mapp*. 2021;42:1034–1053. <https://doi.org/10.1002/hbm.25276>